U.PORTO

FEUP FACULDADE DE ENGENHARIA UNIVERSIDADE DO PORTO

ICBAS INSTITUTO DE CIÊNCIAS BIOMÉDICAS ABEL SALAZAR SCHOOL OF MEDICINE AND BIOMEDICAL SCIENCES

Dissertation for Masters Degree in Molecular Bioengineering

Saccharomyces cerevisiae identification in microfluidic devices using peptide nucleic acid fluorescence *in situ* hybridization (PNA-FISH)

André Miguel Santos Ferreira

Supervisor: **Prof. Nuno F. Azevedo**

Co-Supervisor: **Prof. João M. Miranda**

Developed in:

Faculty of Engineering of University of Porto
Laboratory for Process Engineering, Environment, Biotechnology and Energy
Transport Phenomena Research Center

February, 2022

This dissertation was supervised by:

Professor Nuno Filipe Azevedo, PhD

Faculty of Engineering of University of Porto

Laboratory for Process Engineering, Environment, Biotechnology and Energy

Professor João Mário Miranda, PhD

Faculty of Engineering of University of Porto

Transport Phenomena Research Center

The host institutions of this dissertation were:

FEUP – Faculty of Engineering of University of Porto

LEPABE – Laboratory for Process Engineering, Environment, Biotechnology and Energy

CEFT – Transport Phenomena Research Center

The research described in this dissertation was financially supported by:

i) Base Funding - UIDB/00511/2020 of the Laboratory for Process Engineering, Environment, Biotechnology and Energy – LEPABE - funded by national funds through the FCT/MCTES (PIDDAC);

ii) Base Funding – UID/EMS/00532/2020 of the Transport Phenomena Research Center – CEFT – funded by national funds through the FCT/MCTES (PIDDAC);

iii) Projects POCI-01-0145-FEDER-031011 (μFISH), POCI-01-0145-FEDER-029961 (ColorISH) and PTDC/QEQ-FTT/427/2014, funded by FEDER funds through COMPETE2020 – Programa Operacional Competitividade e Internacionalização (POCI) and by national funds through the FCT/MCTES (PIDDAC);

iv) FCT – Fundação para a Ciência e a Tecnologia (Scholarship SFRH/BPD/98525/2013) and Project NanoDiaBac (ENMed/0003/2014).

"Success is not final, failure is not fatal.
It is the courage to continue that counts."
— Winston Churchill

Acknowledgments

First and foremost, I cannot thank my supervisors enough, Professors Nuno F. Azevedo and João M. Miranda, for opening the door for this project, for all their guidance, knowledge and patience. It is a privilege to witness your combined expertise in PNA-FISH and microfluidics. My deepest gratitude.

A sincere word of appreciation to the entire LEPABE team in lab E007. I would like to specially acknowledge Laura Cerqueira, Andreia Azevedo, Rita Santos, Luciana Gomes, Anabela Borges and Nuno Guimarães, for all their help and know-how in all things FISH related. The same gratitude is extended to the CEFT team in lab E103, in particular to João Carneiro and Tânia Dinis, for sharing knowledge and laughs.

To Daniela Moreira, who laid the foundation for the work presented in this dissertation and guided me through the first steps in combining FISH with microfluidics, thank you!

To my friends, both old and new, to M&B, thank you for *always* sticking with me. I am grateful to know that your names would not fit in one page. Still, I would like to acknowledge the little ones, José, Pedro, Carolina and Alice: welcome to the team!

My gratefulness also goes to my brother Nuno, to Aile and Emily, for all their joy and support. Maybe these pages might help to put Emily to sleep.

To Rita, thank you for being by my side, while also lovingly pushing me forward. I hope to do the same for you.

Finally, I would like to dedicate this work to my parents, Albertino Ferreira and Albertina Tarrio, for their unconditional love and support. I love you both and I hope to make you proud. Obrigado por tudo.

Abstract

Yeast fermentation has been utilized for food and beverage production for centuries, although the exact process was not recognized until the middle of the 19th century. The growing knowledge about yeasts has allowed industries to effectively control the fermentation by regulating both physiology and concentration of yeast in reactors. Both constant evolution of food and beverage industries and growing demand in product quality have ultimately led to a need of new methodologies capable of identifying and quantifying fermentation yeasts, such as *Saccharomyces cerevisiae* (*S. cerevisiae*), while ensuring that no spoilage yeast is present in the reactor and therefore guaranteeing the quality of the final product.

As such, there is a window of opportunity for the development of new screening techniques to tackle the most imperative demands by the above-mentioned industries: speed, specificity, cost and ease of application to different microorganisms. This project aims to develop a low-cost microfluidic device, a system renowned for its ease-of-use and quick results, where *S. cerevisiae* cells would be retained and then detected by a method well-known for its outstanding specificity, peptide nucleic acid fluorescence *in situ* hybridization (PNA-FISH).

Several microchannels with different trapping array configurations (designed with computational fluid dynamics - CFD) were prepared using polydimethylsiloxane (PDMS) via a combination of microfabrication methods, namely photolithography and soft lithography. Then, parameters such as hydrophilicity, flow rate and cell concentration were optimized until optimal retention efficiency of *S. cerevisiae* was achieved. Also, a PNA-FISH protocol was developed and optimized for the specific detection of *S. cerevisiae* in a microfluidic environment. Finally, PNA-FISH and microfluidics were combined and the presence of the intended fluorescent signal was assessed in cells trapped in these microchannels. By combining the advantageous characteristics observed in each microchannel, it was possible to propose a new design capable of improving cell retention efficiency.

The proposed integration of PNA-FISH and microfluidics might tackle the mentioned obstacles which currently hinder significant scale-up of processes essential to fermentation-based industries, providing an efficient and yet cost-effective method for detection and quantification of yeasts such as, but not limited to, *S. cerevisiae*.

Resumo

A fermentação de leveduras para produção de alimentos e bebidas tem sido aplicada ao longo de vários séculos, embora o seu mecanismo só tenha começado a ser estudado desde meados do século XIX. O crescente conhecimento sobre leveduras tem permitido às indústrias controlar a fermentação através da regulação da fisiologia e concentração de leveduras presentes nos reatores. A constante evolução da indústria alimentar e a crescente exigência na qualidade dos produtos resultantes geraram a necessidade da criação de novas metodologias capazes de identificar e quantificar leveduras fermentadoras, como a *Saccharomyces cerevisiae* (*S. cerevisiae*), enquanto se garante que leveduras deteriorantes não estão presentes na mistura, assegurando assim a qualidade do produto final.

Verifica-se assim a existência de uma janela de oportunidade para a criação de uma técnica de deteção capaz de responder às necessidades das indústrias baseadas em processos de fermentação: rapidez, especificidade, custo e facilidade de aplicação em diferentes microorganismos. Este projeto pretende construir um dispositivo de microfluídica, reconhecido pelo seu fácil manuseamento e rápido fornecimento de resultados, onde as células *S. cerevisiae* serão retidas e posteriormente detetadas por uma metodologia caracterizada por atingir uma elevada especificidade, a hibridização *in situ* fluorescente com recurso a ácidos nucleicos peptídicos (PNA-FISH).

Vários microcanais com diferentes configurações na zona de retenção (projetadas com recurso a fluidodinâmica computacional - CFD) foram construídos em polidimetilsiloxano (PDMS) através de uma combinação dos métodos de microfabricação, fotolitografia e litografia suave. Posteriormente, parâmetros como a hidrofilicidade, velocidade do caudal e concentração celular foram modificados até ser atingida uma eficiência ótima de retenção de *S. cerevisiae*. O protocolo de PNA-FISH foi otimizado por forma a atuar em ambiente microfluídico. Por fim, as metodologias de PNA-FISH e microfluídica foram combinadas e a presença de sinal fluorescente foi observada em células retidas nos microcanais. Combinando as características vantajosas de cada microcanal, foi possível propor uma nova configuração capaz de melhorar a eficiência de retenção celular.

A integração de PNA-FISH e microfluídica proposta poderá resolver os obstáculos previamente referidos que dificultam o *scale-up* de procedimentos cruciais para indústrias baseadas em processo fermentativos, proporcionando um método eficiente

e de baixo custo para a deteção e quantificação de leveduras como, mas não limitado a, *S. cerevisiae*.

Table of contents

List of figures

List of tables

List of abbreviations

CFD	Computational fluid dynamics
DNA	Deoxyribonucleic acid
FISH	Fluorescence *in situ* hybridization
FITC	Fluorescein isothiocyanate
FVM	Finite volume method
GRAS	Generally regarded as safe
G-2A	Green excitation longpass
HPLC	High-performance liquid chromatography
LNA	Locked nucleic acid
LOC	Lab-on-a-chip
MALDI	Matrix-assisted laser desorption ionization
MS	Mass spectrometry
OD	Optical density
PBS	Phosphate buffer saline solution
PC	Polycarbonate
PCR	Polymerase chain reaction
PDMS	Polydimethylsiloxane
PE	Polyethylene
PGMEA	Propylene glycol methyl ether acetate
PMMA	Polymethylmethacrylate
PNA	Peptide nucleic acid
PVC	Polyvinylchloride
PYCC	Portuguese yeast culture collection
RAPD	Random amplified polymorphic DNA
RFLP	Restriction fragment length polymorphism
Re	Reynolds number
rRNA	Ribosomal ribonucleic acid
SA:V	Surface-area-to-volume ratio
Tm	Melting temperature
TOF	Time of flight
YEPD	Yeast extract peptone dextrose
2'-F RNA	2'-deoxy-2'-fluoro-ß-D-ribonucleic acid
2'-OMe RNA	2'-O-methyl ribonucleic acid

List of notations

ρ	Density	kg/m^3
v	Flow speed	m/s
l	Characteristic linear dimension of the flow	m
η	Fluid dynamic viscosity	kg/(m.s)
W	Microchannel width	m
H	Microchannel height	m
d	Distance traveled by a particle	m
D	Diffusion coefficient	m^2/s
t	Time duration	s
k_B	Boltzmann constant	$1.38 \times 10^{-23}\ m^2\ kg\ s^{-2}\ K^{-1}$
T	Absolute temperature	K
r	Radius of spherical particle	m
ΔG	Gibbs free energy change	Kcal/mol
ΔH	Enthalpy change	Kcal/mol
ΔS	Entropy change	Kcal/K
Tm	Melting temperature of DNA duplexes	ºC
Tm PNA	Melting temperature of PNA/DNA duplexes	ºC

I. Work outline

1. Framework
2. Aim
3. Dissertation outline

1. Framework

Efficient detection of microorganisms is vital for the food industry, particularly in fermentation-based processes where microbial presence must be closely regulated to achieve the desired product properties[1]. Although conventional culture-based methods are still considered the gold standard, these methods are time-consuming and generally are not able to provide results on a timely basis, thus limiting their ability to protect consumers from potential hazards[2].

Molecular techniques such as fluorescence *in situ* hybridization (FISH) are capable of providing rapid and highly specific results for cellular detection[2], which is particularly suitable for fermentation-based industries[3]. Using FISH employing nucleic acid mimic (such as peptide nucleic acid - PNA) probes allows for a faster and more specific hybridization of the probe to the targeted site when compared to the use of regular deoxyribonucleic acid (DNA) probes[4, 5]. However, PNA probes are more expensive than DNA probes[6] and molecular techniques such as FISH require a sample pre-enrichment step to ensure a minimum number of target cells to be detected, a process that typically takes at least one working day[2].

Microfluidic systems are capable of increasing the concentration of microorganisms in a predetermined location, hence bypassing the pre-enrichment step, allowing the time consumed during the entire procedure for cell identification to be reduced to the time of the technique alone[7]. The strategy adopted to concentrate cell suspensions depends on the cell adherence to the material, with trapping mechanisms being mandatory in the case of non-adherent cells[8]. These miniaturized devices lower the cost per test (since the amount of materials and reagent consumption decreases when scaling down the assay volume), reduce the amount of laboratory equipment/space needed and provide higher sensitivity and portability[9].

As such, application of FISH methodology using PNA probes (PNA-FISH) inside microfluidic devices can be a useful tool for analytical and diagnosis assays, as these devices are able to surpass the aforementioned PNA-FISH limitations for wide industrial use, namely by lowering the complexity of the procedure[10] and reducing the necessary amount of expensive PNA probes[6].

2. Aim

This masters dissertation aims to create a lab-on-a-chip (LOC) device capable of trapping and detecting targeted yeasts to be primarily used by fermentation-based industries, while acknowledging the possibility to eventually adapt the resulting device to detect additional microorganisms and allow its use by other food-based industries, as well as research and medical fields.

Although PNA-FISH integration with microfluidic devices is not a new concept[11, 12], this project evaluates new microchannel designs specifically for yeast cells, with an emphasis on cell retention efficiency and on simplification of the PNA-FISH procedure while ensuring the high sensitivity characteristic of this method. *Saccharomyces cerevisiae* (*S. cerevisiae*) is selected as a case study since it is a common yeast relevant for several types of food industries[13].

As such, the PNA-FISH method based on the protocol provided by Perry-O'Keefe *et al.* (2001)[14] must be adapted to be applied in a scaled-down system. Different parameters must be tested, namely temperatures, solution exposure times and reagent volumes, to determine which values present a better compromise between time, specificity and industrial viability of the process.

The microchannel designs provided by Moreira (2014)[15] must be evaluated according to their ease of fabrication and use, as well as their inherent entrapment capabilities, through a combination of computer simulations (computational fluid dynamics - CFD) and real-time scenarios. Microchannels that demonstrate promising results will be selected for subsequent experiments.

If needed, the microchannel fabrication methodology as described by Choi *et al.* (2012)[16], as well as handling of the resulting microchip system, may be altered. In particular, surface properties of microchannels may be subjected to oxygen plasma treatment, allowing the resulting microchannel to acquire hydrophilicity and thus reducing entrapment of air bubbles and clogging[17].

In the later stage of this work, cell behavior inside the microchannels will be accessed under several parameter changes, mainly cell concentration and fluid flow rate, while evaluating retention efficiency of the microchannel designs. Finally, PNA-FISH procedure will be applied to cells retained in microchannels.

3. Dissertation outline

This masters dissertation is structured into 5 chapters and an appendix.

The current Chapter I (Work outline) is an introductory note to the overall background, objective and structure of the dissertation.

Chapter II (Literature review) provides the background information available for this work. A brief introduction to fermentation-based industries is included, justifying the value offered by this project. An overview of the targeted organism *Saccharomyces cerevisiae* is also featured. Finally, overall concepts of molecular nucleic acid-based detection methods, nucleic acid mimics and microfluidics are presented, with emphasis in fluorescence *in situ* hybridization, peptide nucleic acids and microfabrication methodologies.

Chapter III (Materials and methods) provides information about the material and methods used throughout the project that, in junction with protocols available in appendix, allows replication of the procedures applied during this project and acquisition of similar results.

Chapter IV (Results and discussion) presents results arranged in temporal order, thus allowing to draw conclusions from each set of experiments and to adopt the optimal parameters before continuing to the subsequent assay. Each experiment is followed by a discussion of the obtained results.

Chapter V (Conclusions and future work) concludes this masters dissertation by summarizing the results and following overall discussion, providing the final set of parameters optimized for the inclusion of PNA-FISH in a microfluidic environment. Also, an outline for continuation of this project is provided.

An appendix is also provided, with protocols for YEPD mediums, FISH solutions and further material supporting the obtained conclusions.

II. Literature review

1. Fermentation-based industries
2. Current detection and quantification methods
3. Molecular acid-based detection methods
4. Microfluidics

1. Fermentation-based industries

The use of fermentation by microorganisms such as bacteria, yeasts and fungi in food processes has long been explored by humans[18]. Still, in comparison, the understanding of the biological mechanism behind such processes is fairly recent, with Antoni van Leeuwenhoek's yeast observations in the 17th century and Lavoisier scientific studies on alcoholic fermentation in the 18th century[19]. These studies were then continued by several renowned scientists such as Joseph-Louis Gay-Lussac, Charles Cagniard de la Tour and Louis Pasteur[20, 21]. While fermentation processes have been greatly improved over the years, its scale-up to industrial levels is still problematic, as guaranteeing an homogeneous reaction condition to maintain the final product quality and integrity is quite challenging, mainly due to the lack of effective monitoring and control procedures[22].

1.1. *Saccharomyces cerevisiae*

Transformation of grapes into wine, cereals into beer and bread baking are possibly the oldest documented fermentation processes[23]. In all these fermentation processes, yeast species such as *Saccharomyces cerevisiae* (*S. cerevisiae*) have been shown to play a vital role[23].

S. cerevisiae is a species of yeast, diplontic, both easily obtainable and reproducible[24]. It is a generally regarded as safe (GRAS) organism and therefore is widely used in biological studies, usually as surrogate for more dangerous microorganisms[24]. In fact, *S. cerevisiae* has become increasingly important over recent years in biotechnology as a model organism, being the best characterized eukaryotic microorganism and also allowing genetic modifications by recombinant deoxyribonucleic acid (DNA) technology[24].

Nonetheless, *S. cerevisiae* is still mostly known for its use in both food and beverage industries[24]. In fact, it is regarded as the main organism applied in wine and beer production due to its high alcohol and sulfur dioxide levels tolerance and vigorous (yet predictable) fermentation capacities[25]. It is also known to be essential in bread baking process, where it plays a pivotal role in the rising action of the dough by generating CO_2 and in the production of several aroma compounds[26].

Detecting and quantifying *S. cerevisiae* can be particularly problematic in fermentation industries: while in non-fermented foods any yeast can have an undesirable effect on the food sensorial properties and is therefore regarded as

spoilage yeast, in fermented products there is a predetermined amount of yeast that is beneficial to the process (as the metabolites produced contribute to the flavor) and thus discernment of a spoilage yeast is challenging[27].

This obstacle is emphasized in fermented beverages, where alcoholic fermentation occurs in presence of yeasts and there is a need to effectively determine whether the amount and yeast species is beneficial or detrimental to the fermentation process[28]. In fact, if spoilage yeasts are present in the mixture, stored wines may develop a clouded color, films, sediments and/or gas, ultimately producing a wine with unintended odors and flavors[28]. The importance of monitoring spoilage yeasts has been increasing over the years, as quality winemaking favors minimal use of preservatives (such as benzoic acid or sulphur dioxide) that are used to prevent any flavor alteration in the final product[29].

Considering the aforementioned obstacles, it is of the upmost importance to develop a detection method that allows effective differentiation between fermenting and spoilage yeasts, ensuring the microbiological quality of the resulting products.

2. Current detection and quantification methods

2.1. Conventional phenotypic methods

Differentiation of microorganisms via microscopic and biochemical tests is a conventional, long-time used method in fermentation-based industries, relying on the recognition of specific observable features in a predetermined culture media, such as morphology, development and biochemical or physiological properties resulting from gene expression[30-32]. Although these tests are fairly simple to execute, they are usually time-consuming and heavily rely on the ability of trained technicians to effectively identify the presence and nature of the organism[33, 34]. These setbacks might explain why culture-based differentiation methods are not routinely used in food and beverage industries, in favor of molecular-based methods[35].

2.2. *S. cerevisiae* Isolation and growth in selective media

As most yeasts, *S. cerevisiae* growth seldom occurs in the absence of either molds or bacteria and thus selective media that only allow yeast growth while suppressing other microorganisms are used for *S. cerevisiae* recovery[36]. Knowing that yeasts are generally capable of withstanding pH levels and water activity that inhibit bacterial growth, these media, such as glucose-peptone-yeast extract, are

acidified and osmotic to a point that only acid resistant and osmotolerant yeasts (as is the case with *S. cerevisiae*) are able to grow[36]. Also, to selective isolate particular groups of yeast species, the ideal incubation temperature for a specific yeast strain is used (37°C for *S. cerevisiae*)[36].

3. Molecular and mass spectrometry based methods

As previously stated, despite their low cost and ease of use, conventional culture-based methods are time-consuming and the obtained results are often not as accurate or as useful as intended[28]. Hence, several immunological and molecular-based methods have been applied to food and beverage industries, taking advantage of their rapid detection and enumeration capabilities. With knowledge that the genetic material of each organism is unique and presents species specificity, the design of oligonucleotides that hybridize specifically to predetermined sequences of a certain target has been the basis of powerful molecular approaches.

Polymerase chain reaction-based methods in particular, such as polymerase chain reaction (PCR)-amplified ribosomal DNA, restriction fragment length polymorphism (RFLP) of mitochondrial DNA and random amplified polymorphic DNA (RAPD), have been frequently applied to yeast detection in fermentation processes[37-39]. These methods are based on the amplification and detection of microbial nucleic acids in samples taken during the fermentation process.

The PCR procedure comprises a three-step cycling process: denaturation of double-stranded DNA either by physical or chemical means (usually heating is sufficient); annealing of two oligonucleotide primers to the target DNA, flanking the region of interest; primer extension by the enzyme DNA polymerase, which adds nucleotides complementary to those in the unpaired DNA strand onto the annealed primer[40]. This newly synthetized sequence can then serve as a template for the next cycle and the number of DNA strands doubles upon completion of each cycle[40].

Other than PCR-based methods, there are additional molecular processes allowing effective identification of specific yeast genotypes without requiring DNA amplification. For instance, matrix assisted laser desorption/ionization (MALDI) procedures used in combination with time of flight (TOF) and mass spectrometry (MS) have been shown to be suitable for fast and secure identification of microorganisms[41]. Succinctly, in MALDI-TOF MS the targeted microorganisms undergo a thermal degradation and the resulting molecules are cleaved at their frailest

points, producing volatile fragments from which a pyrolysis mass spectrum is obtained by mass spectrometry and subsequently analyzed as a chemical fingerprint of the yeast[41]. Another molecular-based method that has been considered ideal to be applied in these industries is fluorescence *in situ* hybridization (FISH).

3.1. Fluorescence *in situ* hybridization

Fluorescence *in situ* hybridization (FISH) is a nucleic acid-based methodology introduced in the late 1980s that allows an efficient detection and localization of specific nucleic acid sequences by marking the target site with a complementary oligonucleotide probe covalently linked at the 5'-end to a fluorescent dye molecule[42]. The targeted sequences of FISH probes are typically located in the ribosomal ribonucleic acid (rRNA) since these structures are quite stable, found in all living organisms with high copy numbers (up to 100 000 per cell) and their sequence domains are both variable and highly conserved[42, 43]. Since Stender *et al*. (2001)[44] used FISH for rapid monitoring of lactic acid bacteria and detection of slow growing yeast in the wine industry, this methodology has become widely recognized for its advantages in fermentation-based industries, being capable to match the reliability of molecular methods[43] with the ability to provide directly visible results[45].

FISH methodology is usually composed by three main steps: fixation/permeabilization, hybridization and washing (Figure 1)[42]. The first step, fixation and permeabilization, is based on the application of chemical agents that guarantee preservation of cellular structure and easier access of the hybridization solution compounds to the targeted sites[46]. An efficient fixation ends all enzymatic and other metabolic activities, in this way preventing autolysis and maintaining cellular morphology[47]. Still, since over-fixation may lead to the unintentional formation of fixation artifacts and thus loss of the subsequent signal and/or increased nonspecific background, a compromise must be attained in how intensive the fixation step is[48]. Fixative agents such as glutaraldehyde or formaldehyde are used in FISH to promote cross-linking between proteins[49]. Although there is still no standard fixation protocol for microorganisms, a polymerized form of formaldehyde, paraformaldehyde, is preferred for most FISH procedures since it is a well-known small molecule able to quickly penetrate cellular structures and effectively fixate nucleic acids, while dismissing the need for other additives[49, 50].

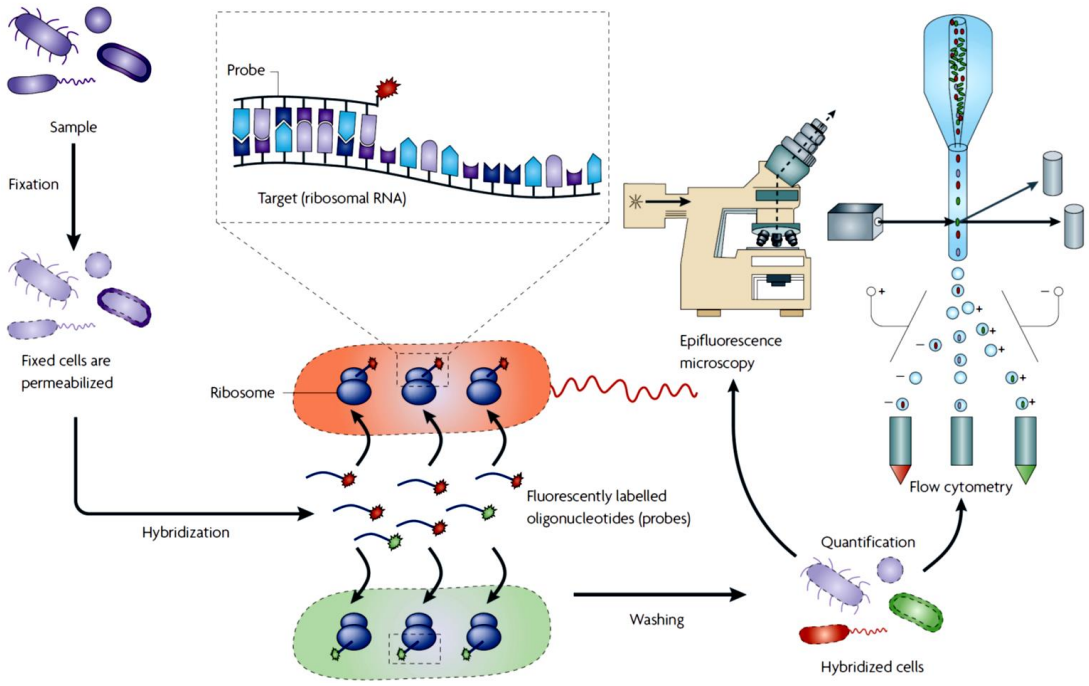

Figure 1 - Basic steps of fluorescence *in situ* hybridization procedure

Cells are first fixed and permeabilized to allow the hybridization step, where a fluorescently-labeled probe will complement the targeted sequence. A washing step is required to remove non-hybridized probes. Labeled cells can then be quantified via fluorescence microscopy or flow cytometry. Figure from Amann *et al.* (2008)[42].

Permeabilization comprises the removal of free water from tissues, forcing hydrophobic chemical groups into closer contact with each other and thus stabilizing hydrophobic bonds, which, besides contributing to the maintenance of an uninjured morphological structure of the target cells throughout the process, ultimately allows diffusion of labelled oligonucleotide probes until they reach their targeted sequences in the intracellular rRNA[42, 51]. Cell membrane permeabilizing agents can be either organic solvents or detergents[52]. Organic solvents are capable of causing precipitation of proteins and carbohydrates, as well as dissolving lipids present in the cell wall[52]. Alcohols such as methanol, ethanol or acetone are the most universally used organic solvents[49]. Meanwhile, detergents such as Triton-X and Tween 20 are used after fixation with cross-linking agents, being able to solubilize phospholipids from the membrane[52]. However, since detergents are non-selective in nature, extraction of proteins along with the lipids may occur and so a compromise in the concentration of detergent used has to be achieved[52]. Also, for microorganisms with cell walls containing thick peptidoglycan layers or walls of high proteinaceous nature, lysozyme or proteases may be used for their permeabilization, respectively[42].

Following the fixation/permeabilization step, hybridization entails incubation of targeted microorganisms with a fluorescently-labeled probe, whose oligonucleotides

are complementary to the targeted sequence[45]. The solution containing target cells and probe is exposed to well-defined parameters (time of hybridization, temperature, pH, ionic strength and denaturant solvent concentration) as a way to allow diffusion of the probe through the intracellular environment and to induce denaturation of nucleic acid strands, making them available to anneal with the complementary probe[6, 45]. Optimization of such parameters is therefore crucial to achieve ideal results from the FISH procedure[6]. Fluorescently-labeled probes are also essential for an effective FISH procedure, generally targeting a sequence in 16S or 18S rRNA, although it is also possible to target sequences in larger rRNA sub-units[43]. rRNA is an ideal target due to its abundance in most cells (there are nearly 200 000 ribosomes in a single *S. cerevisiae* cell)[53], which amplifies the fluorescent signal. In addition, rRNA sequences are recognized as phylogenetic markers due to the apparent lack of lateral gene transfer and a sufficient length of about 1500 (16S sequence) or 3000 nucleotides (23S sequence) in Bacteria or Archaea[43] and 1800 (18S sequence) or 3400 nucleotides (26S sequence) in Eukarya[54, 55]. If the probe is properly designed and the protocol is optimized and still the obtained fluorescence signal remains insufficient or non-existent, the cause of FISH procedure failure usually relies on ineffective cell permeabilization, low cellular ribosome content or inaccessibility to the probe binding site inside the ribosome[42].

Finally, the washing step comprises the removal of non-hybridized or partially hybridized probes, preventing occurrence of false positive signals on the final results[45]. After these steps, the sample can be quantified via fluorescence microscopy or flow cytometry, depending on the target sequence and the parameters intended to be observed[45].

Since its development, FISH technique has been useful to a wide range of applications, for example to detect pathogenic agents in clinical samples[56], as a biomarker in cancer progression[57], in the characterization of community structures and diversity of natural habitats[42, 58], to evaluate gene presence and expression[59] and to assess chromosome stability in stem cell research[60], among other uses. This large variation of applications requires FISH procedure optimization for each of them by altering some key parameters, such as time, temperature, pH values and concentration of reagents on any of the three main steps.

3.2. Nucleic acid mimics

Soon after the description of the FISH technique for microbial identification[61], nucleic acid mimics (artificially synthesized polymers similar to DNA or RNA) started to emerge as promising factors in cellular detection for both clinical and environmental samples[4].

Peptide nucleic acid (PNA) is one of first developed DNA mimics, although its effective use as a probe for microorganism identification is more recent[62]. Being relevant for this project, PNA characteristics are expanded in the next subchapter.

Another common nucleic acid mimic is the locked nucleic acid (LNA)[6], characterized for its higher thermal stability and improved selectivity, therefore being quite useful in functional genomics and therapeutic applications[63]. LNA stability is a result of its structural conformation, where the sugar is enclosed due to the fact that ribose is linked to a methylene bridge between 2'-oxigen and 4'-carbon atoms[6].

2'-O-methyl ribonucleic acid (2'-OMe RNA), 2'-deoxy-2'-fluoro-ß-D-ribonucleic acid (2'-F RNA) and morpholinos are three other common backbone modified structures demonstrating high affinity, specificity and binding capacity that might become decisive in the development of more robust FISH procedures. Besides these, several other PNA or LNA-modified molecules have also been recently introduced[6].

3.2.1. Peptide nucleic acid

In PNA probes the oligonucleotide bases and the distance between them remains the same as in equivalent DNA probes, while the negatively charged sugar-phosphate backbone of the DNA is substituted by a neutral polyamide backbone (repeating N-(2-aminoethyl)-glycine units linked by peptide bonds)[4]. This change allows the PNA molecule to have a neutrally charged structure and, unlike DNA/DNA duplexes, there is no electrostatic repulsion between PNA/DNA duplexes (Figure 2)[5].

The PNA/DNA duplexes higher stability and consequently higher melting temperatures (Tm - temperature at which one half of the DNA duplex will dissociate to become single stranded) when compared to DNA/DNA duplexes[14] means that while DNA probes require a length of at least 20 to 25 bases to be stable, PNA probes can be significantly smaller (15 bases are sufficient to make a stable PNA probe), which will coincide with higher destabilization by a single-base mismatch and thus improve their binding specificity to the complementary DNA[64]. PNA is also resistant

to enzymatic degradation, as its synthetic structure is not easily recognized by nucleases or proteases[65]. Hybridization with PNA probes requires less salt concentration, providing an environment that promotes destabilization of secondary structures of rRNA and therefore allows easier access to the target sequences[66]. The PNA hydrophobic character associated with its smaller size also promotes its diffusion through cellular membranes and several other lipid-based microstructures[67]. Still, PNA mobility within the cell is more challenging because of the consequent water insolubility that tends to result in molecular aggregation, an occurrence that can be corrected with solubility-enhancing modifications to the PNA molecule[67, 68]. These PNA characteristics imply that PNA-FISH has significant advantages over regular FISH, such as excellent signal-to-noise ratio, low photobleaching and mild washing procedures[65].

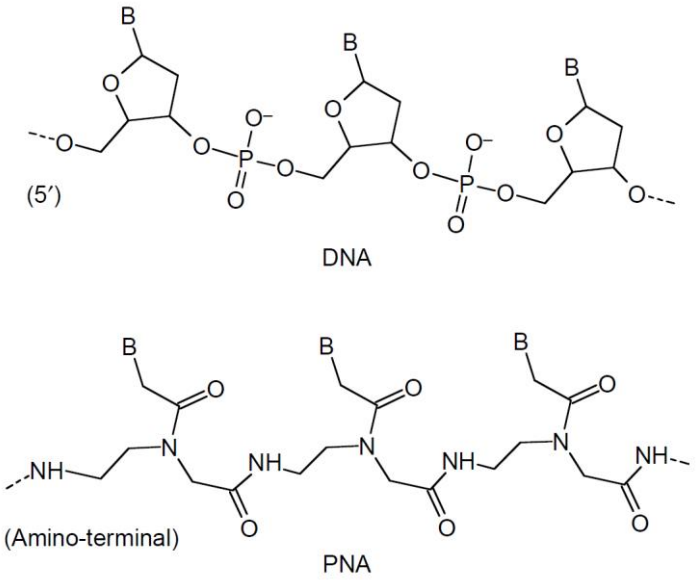

Figure 2 – DNA and PNA molecular structures

While the DNA molecule has a sugar phosphate backbone, in PNA that structure is instead composed by a polyamide chain, removing the negatively charged nature of the DNA while maintaining the space between the nucleotides (represented by the letter B). As a result, there is no electrostatic repulsion between PNA/DNA duplexes. Figure from Nielsen (2001)[5].

3.3. PNA-FISH application at industrial level

As previously stated, identification methods for microorganisms depending on either phenotypic analysis or colony growth on a controlled environment (culture plates) are considerably laborious and technically demanding, usually taking days to provide results[10]. In addition, the lack of specificity resulting of subjective analysis ultimately makes these methods unreliable to be applied at industrial level[69].

While nucleic acid-based methodologies can overcome the specificity and speed problems of conventional methodologies, some barriers remain that hinder their application at industrial level. The multistep protocol needed to perform an efficient FISH protocol takes approximately three hours to be completed, requiring handling by trained professionals and specialized visualization equipment (e.g. fluorescence microscope)[2, 70]. Also to consider, the sample has to contain a high concentration of the target microorganism, otherwise a pre-enrichment step is necessary, further extending the time required for the procedure to a full day[2]. Adding the particular to PNA-FISH setback of expensive probes, the difficulty in applying such procedure at an industrial level is understandable and must be revised[65-71].

The development of a microfluidic system (lab-on-a-chip - LOC) integrated with the PNA-FISH methodology, simplifying and scaling-down the PNA-FISH procedure, is a possible solution to most of the previously described problems. Such scale-down of PNA-FISH will also require an optimization of protocol, specifically regarding the fixation/permeabilization agents used and the duration/temperature applied on each step of the technique. To clarify the advantages of combining PNA-FISH with LOC, microfluidic systems will be discussed in the next subchapter.

4. Microfluidics

Microfluidics refers to the study of devices and methods for controlling and manipulating fluid flows typically at a sub-millimeter scale (down to around 100 nm, were the area of study shifts to nanofluidics)[72, 73]. In a way, the LOC concept aims to efficiently integrate laboratory functions, as is the case with PNA-FISH, on a single chip the size of a few millimeters.

The miniaturization of such procedures allows for a high surface-area-to-volume ratio (SA:V) in microfluidic systems[74], although with the implication that surface forces (e.g. viscosity or surface tension) outweigh volume forces (e.g. inertia or gravity). A large SA:V and low thermal mass makes heat transfer between the fluid and environment more efficient (temperature control is more manageable)[75] and interplay of multiple physical effects such as pressure gradients and capillarity must be attended to[72]. Particularly relevant, the Reynolds number (Re) is a dimensionless number representing the ratio of inertial to viscous forces calculated by the following equation[76]:

$$Re = \frac{\rho v l}{\eta} \quad (1)$$

where density is represented by ρ (kg/m^3), v (m/s) is the flow speed, l(m) is a characteristic linear dimension of the flow and η (kg/(m.s)) is the fluid dynamic viscosity. The characteristic linear dimension of the flow for rectangular microchannels is obtained by the following equation[77]:

$$l = \frac{2WH}{(W + H)} \quad (2)$$

being W (m) the microchannel width and H (m) its height.

Also to consider, sheer stress caused by the fluid being in contact with a stationary surface (wall of the microchannel) leads to the occurrence of a boundary layer where the fluid velocity profile is nearly brought to a rest[78]. As such, maximum fluid velocity is registered away from the walls, at the central axis of the microchannel, resulting in the characteristic parabolic flow profile of microchannels, illustrated in Figure 3[79].

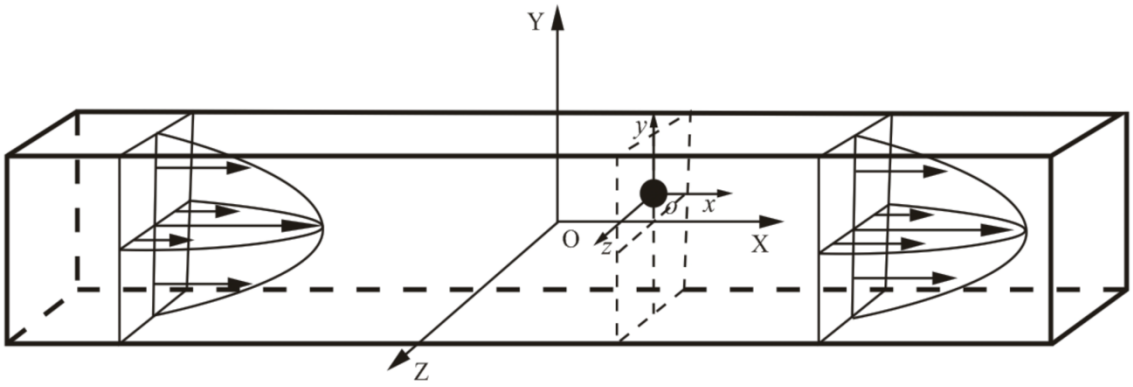

Figure 3 – Schematic illustration of a fully developed parabolic velocity profile in a microchannel

Maximum flow velocity is observed at the central axis of the microchannel, whereas the flow velocity is minimal at the boundary layers near microchannel walls. A spherical particle represented by *o* is positioned at an arbitrary transverse position in the microchannel, showing the transverse component of the hydrodynamic force exerted on the particle by the surrounding fluid. Adapted from Wang *et al.* (2017)[79].

The Reynolds numbers in microfluidic environments are small or at least not so large to the point that the convective terms of the Navier-Stokes equation (which describes viscous flows) become relevant[72, 80, 81], which is verified by the laminar flows observed in microfluidic devices (for cylindrical tubes Re <2300 is the threshold for laminar flows, which can be used as an approximate reference for other microchannel geometries)[82, 83]. Consequently, a stream flowing in contact usually does not mix and the fluid particles move in separated layers[82]. A transport

phenomenon that is able to cause mixture of streams in laminar flow is diffusion, where a concentrated solute spreads out over time through random movements until it becomes evenly distributed[82]. Particles present in the fluid obey to a mathematical model that represents random movement of these particles when in suspension, Brownian motion[84]. The distance d (m) traveled by a particle for the duration of t (s) and with a diffusion coefficient of D (m^2/s) is mathematically represented by[84]:

$$d = \sqrt{2Dt} \tag{3}$$

To obtain the diffusion coefficient, hydrodynamic properties of spherical particles in liquids with low Reynold numbers must be attended to, represented by the Stokes-Einstein equation[85]:

$$D = \frac{k_B T}{6\pi\eta r} \tag{4}$$

where k_B is the Boltzmann constant (1.38×10^{-23} m^2 kg s^{-2} K^{-1}), T (K) is the absolute temperature, η (kg/(m.s)) is the fluid dynamic viscosity and r (m) is the radius of the spherical particle.

In view of the exceptional complexity of fluid movement observed in microfluidic environments, there is a need to apply computer simulations to predict such flow movements (discussed in the next subchapter). Still, these devices have multiple characteristics that pose as great advantages for the present project, namely the wide availability of methods for fabricating both individual and integrated flow configurations[80], the ability to manipulate and detect samples with volumes in the microliter range[86], the possibility of replicating dynamics of a single microchannel in multiple microchannels organized into sub-networks[87] and the fact that these systems are relatively cheap, portable and capable of performing simple analytical tasks, with great potential for chemical and biological processes[72].

Application of a microfluidic system should enable execution of PNA-FISH by professionals not necessarily familiarized with this methodology. The total cost of the procedure is also expected to decrease, as less concentration of reagents will be needed, which is especially useful when considering the higher cost of PNA probes (when compared to DNA probes). Additionally, since cells are expected to be concentrated within the microchannels, mainly confined to the trapping array section, the sample enrichment step (usually required in FISH to increase cellular concentration and therefore avoid false negative results) can be bypassed and the

results will be obtained in a considerably shorter time. It is worth mentioning that successful integration of FISH into a LOC is already documented for the detection of chromosomal changes in cancer cells[88] but the introduction of the significantly higher stability and specificity of PNA probes can further improve this method.

4.1. Computational fluid dynamics

While replicating the LOCs is usually not expensive (depending on the material used), producing the necessary master molds has a significantly higher cost[89]. Also, the previously mentioned high surface-area-to-volume ratio in microfluidic channels means that surface forces prevail over volume forces and therefore unexpected fluid behavior may occur, resulting in a difficult understanding of fluid behavior without proper visualization methods[72, 80, 81]. Considering these hurdles, it has become standard procedure to test every microchannel design in a computer simulation before producing the master mold, in a field known as computational fluid dynamics (CFD)[90].

CFD is a branch of fluid mechanics that, using algorithms, can analyze and solve problems related to fluid flows[91]. First, microchannels are designed using computer aided design software, e.g. Autodesk AutoCAD[92]. These geometries are then entered into fluid simulation software, Ansys Fluent, that follows a series of steps: the geometry is recognized and its boundaries, such as inlet/outlet conditions and wall properties, are defined; the geometry is divided into small computation cells, in a process named mesh generation (a more refined mesh leads to an improved numerical solution of the equation); models for turbulent and laminar flows as well as fluid properties (viscosity, density, among others) are set; finally, the solver (pressure-based or density-based) and quality of an acceptable solution in terms of convergence criteria are defined, resulting in an image representing the predicted fluid flow through the microchannel design[92]. This last step is done by an iterative solution method, where the equation sets variables (e.g. pressure and velocity) that are solved sequentially and repeatedly until a converged solution is obtained[92].

The numerical solution technique used by Ansys Fluent to provide CFD results is the finite volume method (FVM). FVM divides the inputted geometry into a mesh, from which each of the cells (named control volumes) will have a corresponding grid point (node)[93]. A smaller control volume leads to lower magnitudes of error but, since a grid too fine will increase the computational effort and slow down the simulation, a compromise must be made to determine a control volume at which results are obtained in a timely manner and yet with a small margin of error[93].

This procedure allows selecting a range of possible successful microchannels before having to produce and test them in real-life conditions (improving time and cost efficiency of the project) and to visualize the fluid flows inside the different microchannel configurations (allowing further understanding of possible variations capable of producing an improved microchannel design).

4.2. Trapping arrays

To guarantee that the target microorganism is retained in significant concentration inside the microfluidic system throughout the FISH procedure, numerous trapping array configurations must be designed and tested. Although several complex trapping methods are available for use in microfluidic systems (e.g. acoustic, electric or magnetic trapping)[94], in order to keep the low cost of the resulting microchannel while maintaining its simplicity of construction and use, the most common cell trapping method, hydrodynamic trapping, is preferred for this project[77]. Hydrodynamic cell trapping consists in designing narrow sections in a limited microchannel area, while not completely obstructing the fluid flow throughout the microchannel[77].

Microorganisms can be sorted according to their size either by microfluidic filters incorporated into the microchannel[95] or through the introduction of a porous bed methodology[96]. Alternatively to these methods, considering that *S. cerevisiae* consistently presents a diameter of 5 to 10 μm[97],a simple barrier structure with openings of 5 μm is usually capable of trapping these microorganisms, while adding wider openings can ensure that the microchannel is not completely blocked by accumulation of microorganisms nor other particles[94]. The efficiency of well-known barrier/pillar-based designs, such as horseshoe-shaped traps and dams with narrowing sections, has already been demonstrated by several authors[94, 98, 99], being ideal for this project for their ability to maintain microorganism retention even when fluid flow is stopped (necessary in the PNA-FISH protocol for application of fixation/permeabilization, hybridization and washing steps)[94].

The number, size, shape and positioning of the trapping arrays are key parameters that could determine the success of the proposed method and it is therefore essential to perform extensive testing of several trap designs in CFD before producing the LOCs molds. There is also a need to determine a compromise between pillar size and microchannel depth, since pillars are liable to bend if they are either too tall or too thin and a failure of even a few pillars may be crucial to the

entrapment efficiency[100]. Only then the proposed microchannels will be constructed through microfabrication.

4.3. Microfabrication

As the name implies, microfabrication is a fabrication technique through which three dimensional microstructures (in scale lengths less than a millimeter, down to 100 nm) are constructed[73, 101]. Both fabrication technique and material used must be chosen accordingly to the intended application, as a way to keep the procedure at a low cost while not compromising its effectiveness[102].

Replica molding is a microfabrication process that consists in manufacturing a hardened chip by pouring an elastomeric material in liquid form over a master mold with topographical features of the intended design[103, 104]. Fabrication of LOCs via replica molding usually follows a procedure adapted from McDonald *et al.* (2002)[105], where photolithography and soft lithography techniques are applied to produce the master mold and elastomer microchips, respectively[104].

First, the master mold is manufactured, usually by photolithography, a common microlithographic technique[106]. A silicon wafer is spin-coated with SU-8, a photocurable epoxy widely considered to be ideal for microfluidic molds as it has high lithographic contrast, enabling the production of high resolution structures[107]. It is possible to control SU-8 thickness by adapting the spin-coating procedure, which will be reflected on the microchannel depth[107]. Over this SU-8 coated silicon wafer is placed a transparent sheet imprinted with the AutoCAD design, acting as a photomask where the imprinted design (corresponding to the relief structures) will not permit passage of light[16]. The apparatus is then submitted to UV light that passes through the intended photomask sections, generating a cross-linking reaction on the exposed SU-8 regions, ultimately replicating the pattern of the photomask onto the SU-8 (Figure 4 a)[16]. Finally, the non-cured epoxy is removed by an organic solvent such as propylene glycol methyl ether acetate (PGMEA)[108], while small bulges of cured SU-8, corresponding to the relief structures, remain (Figure 4 b)[16].

Using the master mold generated through photolithography, it is possible to create several microchips via soft lithography technique. Soft lithography is a strategy based on replica molding, allowing the production of an elastomeric block with patterned relief structures on its surface[104]. A prepolymer of the elastomer is poured over the master, having the negative structure imprinted on the elastomer surface (Figure 4 c), which is then cured and peeled off (Figure 4 d)[16, 109]. The

elastomeric capability of the block is imperative so that demolding is possible without permanent deformation of the imprinted relief structures[110]. Finally, holes are punched with a needle into the inlets and outlets of each microchannel and the resulting block surface with the imprinted relief structures is covered by a glass slide previously spin-coated with a thin layer of liquid elastomer (with a smaller quantity of curing agent added, therefore this elastomer is less viscous), being that further curing is needed to attain a covalent adhesion between the two surfaces[105, 111].

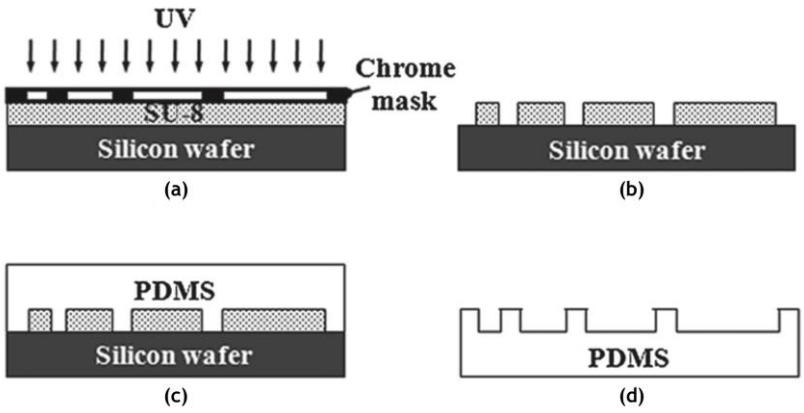

Figure 4 – Schematic representation of the photolithography and soft lithography techniques

Photolithography: (a) UV light passes through a photomask with the imprinted design to cure a SU-8 layer; (b) Uncured SU-8 is removed and relief structures remains over the silicon wafer, completing the master mold construction. Soft lithography: (c) an elastomer in liquid form is poured over the master mold and cured to attain polymeric structure; (d) After curing, the hardened elastomer block is removed from the master mold. Adapted from Choi *et al.* (2012)[16].

4.4. Polydimethylsiloxane

The choice of photolithography/soft lithography microfabrication techniques must be made in conjunction with the selection of the elastomer used to build the block. A variety of polymers are available at a low cost for mass production of LOCs, such as polycarbonate (PC), polymethylmethacrylate (PMMA), polyvinylchloride (PVC), polyethylene (PE) and, more commonly used, polydimethylsiloxane (PDMS) (Figure 5)[112, 113].

PDMS is a compound from the silicones group and considered to be a material of excellence to construct inexpensive LOCs while not compromising their function[114]. Among its several properties, PDMS presents an impressive set of advantages that justify its use in microfabrication: it is isotropic, homogeneous, transparent (down to around 300 nm), thermally stable (can be cured by being subjected to high temperatures), resistant to mechanical stress, biocompatible, has low interfacial free energy, is inert (easily accepts incorporation of other elements), attaches to

non-planar surfaces, is not hygroscopic (does not swell with humidity) and is a considerably cheap material[110, 115]. However, its porous nature means that PDMS is permeable to gas and susceptible to sagging, with higher pressures or even some organic solvents being capable of causing its deformation[115].

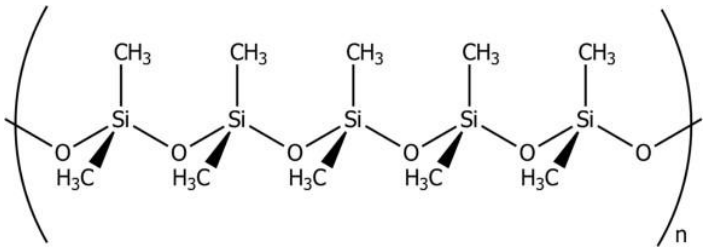

Figure 5 – Polydimethylsiloxane polymeric structure

PDMS empirical formula is $CH_3[Si(CH_3)_2O]_nSi(CH_3)_3$, with *n* being the number of repetitions of the $[SiO(CH_3)_2]$ monomer. Figure from Bowen *et al.*(2012)[113].

The fact that PDMS acts as a viscous liquid (before being hardened into an elastic solid state) allows it to cover the mold, acquiring the microchannel configuration before being removed as a solid chip. The PDMS chemical formula is $CH_3[Si(CH_3)_2O]_nSi(CH_3)_3$, where *n* is the number of units of the repeating monomer $[SiO(CH_3)_2]$ (the higher *n* value, the more viscous and hardened is the resulting PDMS)[116]. Its base monomer is then vinyl-terminated, with methyl-terminated monomers and silicone hydride units. Hardening of the PDMS occurs when it is combined with a curing agent and submitted to curing procedure at 80°C, which causes the crosslinking of the monomer vinyl groups with silicon hydride groups, forming $Si\text{-}CH_2\text{-}CH_2\text{-}Si$ linkages while leaving CH_3 groups exposed in the PDMS surface, which contributes to its highly hydrophobic nature[117]. As a result from this hydrophobicity, filling PDMS microchannels with aqueous solutions can be problematic due to persistence of air bubbles and some organic solvents might even be absorbed by the PDMS[118]. It is possible to alter PDMS surface chemistry by exposing it to energy capable of causing surface oxidation, which can either be done through ultra-violet light[119], corona discharges[120] or, more frequently, oxygen plasma treatment[121].

4.5. Oxygen plasma treatment

Since analysis of biological samples and chemical synthesis usually entails using hydrophobic surfaces[122], plasma oxygen treatment is often applied to attain a hydrophilic PDMS surface[121]. Plasma is a partially ionized gas, meaning that a portion of electrons and ions are free rather than bound to an atom or molecule and, therefore, radical species abound[118]. Oxygen plasma treatment is able to introduce

polar functional groups, mainly silanol groups (SiOH), on the PDMS surface, being these groups that change surface properties from hydrophobic to hydrophilic (Figure 6)[123, 124]. Still, the reactions occurring on the PDMS surface during plasma application are complex and so the mechanism behind surface oxidation is not yet fully understood[118]. This procedure adds capillary effects to the microchannels and reduces any flow hindrance that might otherwise appear, consequently decreasing the occurrence of air bubble immobilization in the microchannel and cellular adhesion to the microchannel surfaces[125, 126].

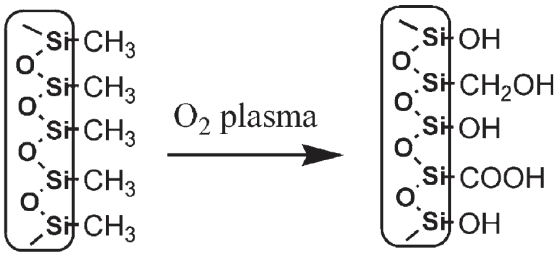

Figure 6 - Schematic of PDMS structural change when submitted to oxygen plasma treatment
The introduction of polar functional groups (SiOH) to the polymeric chains in the PDMS surface allows the acquirement of hydrophilic capabilities. Figure from Wu *et al.* (2007)[123].

The effect obtained by this procedure is not permanent, as normal plasma treated surfaces undergo hydrophobic recovery within a few hours after bonding or even a few minutes if submitted to thermal treatment[127]. Hydrophobic recovery rate is affected by storage conditions such as temperature[128], humidity[129], aqueous fluids[130] and surfactants used to store the PDMS device[131]. The main reason for this hydrophobic recovery relies on the fact that only the PDMS surface is treated, not the entire PDMS bulk[127]. Thus, there is a possibility of reorientation of polar groups from the surface to the bulk[132], diffusion of preexisting low-molecular-weight species also from the bulk to the surface[133] and condensation of preexisting hydroxyl groups[121]. Maintenance of hydrophilic properties may be extended for at least 7 days or more by storing oxygen plasma treated PDMS LOCs in vacuum, low temperatures and/or in water, preventing the reorganization of the silanol group and therefore hindering the hydrophobic recovery processes previously described[127]. While increasing plasma exposure time will also decrease the hydrophobic recovery rate[124], a compromise in the oxygen plasma procedure duration and intensity must be made, since extended plasma treatment may induce formation of undesirable surface cracks[127].

Oxygen plasma treatment is also able to replace the last step of microfabrication, where the PDMS block with the imprinted relief surface would

usually be joined to a glass slide spin-coated with a less viscous PDMS coating and submitted to a curing procedure, creating an irreversible covalent bond between the two surfaces (PDMS-PDMS seal)[111] . Instead, applying the oxygen plasma treatment to both the PDMS block and the uncoated glass slide allows to create a strong and irreversible covalent bond upon joining the two surfaces, since the newly created silanol groups end up condensing with those on the opposite surface (Si-O-Si bonds are created after loss of a water molecule), generating a PDMS-glass seal[134]. This PDMS-glass seal allows to achieve a more reliable microchip construction when compared to that obtained with the PDMS-PDMS seal, which is significantly more susceptible to allow separation of the PDMS block form the PDMS coated glass slide in a destructive peel test[135].

Changes in the obtained hydrophilic nature of the PDMS via the oxygen plasma treatment are often quantified through sessile drop methodology, where a fluid (usually ultrapure water) angle of contact with the PDMS surface is measured[134, 136]. If the contact angle is superior to 90 degrees the surface is considered hydrophobic, whereas a contact angle inferior to 90 degrees indicates that the surface is hydrophilic[137].

4.6. Liquid handling system

Microfluidic systems can also be defined by their liquid handling system. In LOCs, an apparatus consisting of a syringe pump system connected to the microchannel via a PVC tube is commonly used, with the liquid handling system being determined by a pressure driven laminar flow (pressure gradients cause fluid movement)[138]. Furthermore, since oxygen plasma treatment grants the microchannel a hydrophilic nature, significant capillary forces occur and, as a result, the liquid handling system may also be defined by lateral flow[138]. To note, the capillary effect is regulated only by the interplay between the surface tension of the liquid and both the surface chemistry and geometry of the surface, therefore not being possible to control flow velocity when the fluid first enters an hydrophilic microchannel[139].

III. Materials and methods

1. Yeast strain and growth media
2. PNA-FISH
3. Microchannel and trapping array designs
4. Computational fluid dynamic simulations
5. Microfabrication
6. Contact angle measurements
7. Introduction of fluid into microchannels
8. Microchannel retention tests
9. PNA-FISH in microchannels
10. Microscopic visualization

1. Yeast strain and growth media

Saccharomyces cerevisiae strain PYCC 4072 (Portuguese yeast culture collection) was provided by Dr. Manuela Rodrigues from the Biology Department of University of Minho and maintained at -80°C in yeast extract peptone-dextrose (YEPD) medium with the addition of 25% (w/v) glycerol. YEPD medium composition is presented in Appendix I – Table 2. In all YEPD mediums, distilled water is added to achieve the final volume.

S. cerevisiae preculture was prepared according to Larsson *et al.* (1993)[140], by streaking a loopful of biomass obtained from the medium stored at -80°C onto a YEPD-agar plate (YEPD-agar medium composition is presented in Appendix I – Table 3) and the plate was incubated for at least 24 hours at 37°C (FOC 225E Incubator, VELP Scientifica, Usmate, Italy). To prepare liquid cultures, a loopful of biomass was transferred into 100 ml of YEPD medium (not containing glycerol) in a 250 ml Erlenmeyer flask and incubated overnight (approximately 16 hours) at 37°C while mixing at 160 revolutions per minute (IKA KS 130 basic shaker, Vidrolab, Gandra, Portugal), under aerobic conditions, yielding a stationary phase culture[141].

To obtain *S. cerevisiae* in mid-log phase, a sample of the liquid culture obtained overnight was diluted with YEPD medium in a 50 ml falcon until an optical density at 600 nm (OD_{600}) of 0.2 was obtained (V-1200 spectrophotometer, VWR International, PA, USA). After approximately 4 hours, a 0.9 OD_{600} was reached, at which point *S. cerevisiae* is at the mid-log phase with a cell density of 1-5x10^7 cell/ml, according to the growth curve constructed by Lima (2013)[142] (Appendix II – Figure 26). Yeast growth was then stopped by applying the fixation protocol (detailed in the upcoming subchapter III - 2.2).

In microfluidic experiments where non-fixed cells were used, centrifugation was applied as a way to remove the YEPD medium and the resulting pellet was diluted into the same quantity of phosphate buffer saline solution (PBS). PBS composition is presented in Appendix III – Table 4.

2. PNA-FISH

The PNA-FISH protocol used in this project was adapted from the protocols described by Perry-O'Keefe *et al.* (2001)[14], Guimarães *et al.* (2007)[56] and Moreira (2014)[15]. Tables with compositions of FISH solutions (PBS, hybridization solution and washing solution) are presented in Appendix III. In all FISH solutions, distilled water is added to achieve the final volume and, when required, pH levels are adjusted with hydrochloric acid (HCl – 1M) or sodium hydroxide (NaOH – 2M).

2.1. Probe sequence and optimization

The PNA probe targeting *S. cerevisiae* 26S rRNA was designed by Meireles (2012)[143] in PRIMROSE software v2.17[144] and synthesized at Panagene Inc. (Daejeon, South Korea). This probe is connected to an Alexa Fluor 594 dye (red fluorescence), has the sequence AGGCTATAATACTTACC (5' to 3') and was purified at >90% by high-performance liquid chromatography (HPLC). The probe theoretical specificity is 91.1%, calculated as the number of *S. cerevisiae* hits versus total *S. cerevisiae* sequences in the database.

Another PNA probe was ordered from Panagene Inc. (Daejeon, South Korea) with the sequence GACGGGCGGTG (5' to 3') and connected to an Alexa Fluor 488 dye (green fluorescence), being able to target rRNA from Bacteria, Archaea and Eukarya cells.

By examining changes in value of Gibbs free energy during the hybridization reaction, it is possible to estimate the thermal stability (melting temperature - Tm) that will affect the probe affinity to the target[145]. As such, the thermodynamic parameters of both probes are summarized in Table 1:

Table 1 - PNA probes sequencing and thermodynamic parameters

Enthalpy change (ΔH), entropy change (ΔS), Gibbs free energy change (ΔG), melting temperature of DNA duplexes (Tm) and melting temperature of the PNA/DNA duplexes (Tm PNA).

PNA probe sequence (5' to 3')	ΔH (Kcal/mol)	ΔS (Kcal/K)	ΔG (Kcal/mol)	Tm (°C)	Tm PNA (°C)
AGGCTATAATACTTACC	-115	-321.7	-15.26	62.4	66.2
GACGGGCGGTG	-83.7	-220.8	-14.67	72.9	80

Hybridization of the PNA probe targeting *S. cerevisiae* 26S rRNA (red fluorescence) in the parameters used during this project was optimized by Moreira (2014)[15], setting the optimal hybridization temperature at 54 ºC.

The probe targeting rRNA from Bacteria, Archaea and Eukarya cells (green fluorescence) was optimized by testing different hybridization temperatures (51, 53, 55, 57 and 59 ºC) and visually assessing the intensity of the fluorescent signal obtained.

2.2. Fixation and permeabilization

Fixation in suspension was carried out by centrifuging 1 ml of *S. cerevisiae* (in mid-log phase, with 0.9 OD_{600}) at 10 000G for 5 minutes (centrifuge 5418, Eppendorf, Hamburg, Germany) and the obtained pellet was resuspended in 400 µl of 4% (w/v) paraformaldehyde (Acros Organics, Geel, Belgium), followed by incubation for 1 hour at room temperature. After this, permeabilization was carried out by centrifuging the previous solution at 10 000G for 5 minutes and resuspending the pellet in 500 µl of ethanol 50% (v/v), after which cells were incubated for at least 30 minutes at -20 ºC (in these conditions, cells could be stored for up to 6 months).

If hybridization was to be carried out in glass slides (Thermo Fisher Scientific Inc., MA, USA), 30 µl of the previously fixed cell suspension was added to the slides and dried in a drying and heating chamber (FD 23, Binder GmbH, Tuttlingen, Germany), after which hybridization protocol in slides was applied.

Alternatively, fixation/permeabilization could be performed directly on the slide, where 30 µl of *S. cerevisiae* (in mid-log phase, 0.9 OD_{600}) was dispersed onto the well of the slide and dried by flame or in a drying and heating chamber. Then, 40 µl of paraformaldehyde 4% (w/v) was added to the well, followed by an incubation period of 10 minutes at room temperature. After removing the previous reagent with absorbent paper, 40 µl of ethanol 50% (v/v) was added to the well, the slide was incubated for 10 minutes at room temperature and finally the remaining liquid was removed with absorbent paper.

2.3. Hybridization

Hybridization in suspension was performed by dividing the fixed cell suspension into 200 µl aliquots and centrifuging at 10 000G for 5 minutes. The resulting pellet was resuspended in 100 µl of simplified hybridization solution developed by Moreira

(2014)[15] containing the PNA probe (Appendix III – Table 5). For the negative control no probe was added to the hybridization solution.

Hybridization in glass slides was carried out by adding 30 µl of the same simplified hybridization solution (again, with PNA probe for positive results or without PNA probe for the negative control) to each well, covering with 18x18 mm cover slips (Menzel Gläser, Braunschweig, Germany) and incubating for 1 hour at the optimized temperature for the utilized PNA probe (54 ºC for the probe targeting *S. cerevisiae* 26S rRNA, 59 ºC for the probe targeting rRNA from Bacteria, Archaea and Eukarya cells).

2.4. Washing

Following hybridization in suspension, the solution was centrifuged at 10 000G for 5 minutes and the resulting pellet resuspended in 500 µl of washing solution (Appendix III – Table 6). This was followed by an incubation period of 30 minutes at 54 or 59 ºC (depending on the PNA probe used). The solution was then centrifuged with the same parameters previously used and the pellet was resuspended in 500 µl of distilled water, at which point 30 µl of the resulting solution were placed on a glass slide, dried and observed in an epifluorescence microscope (detailed in the upcoming subchapter III - 10).

If hybridization occurred in glass slides, the excess hybridization solution was removed with absorbent paper and the glass slide was incubated in a preheated coplin jar filled with washing solution at 54 or 59 ºC (depending on the PNA probe used) for 30 minutes. After drying the slides were ready to be observed in an epifluorescence microscope (subchapter III - 10).

3. Microchannel and trapping array designs

Microchannel and trapping array designs were provided by Moreira (2014)[15]. The microchannels used have 4 distinct configurations: microchannel 1 is narrow (meaning that its width is constant between the inlet and outlet sections), microchannel 2 is widened at the trapping array section and both microchannel 3 and 4, while narrow at the trapping array section, present a more complex design with double inlets. Using different trapping array configurations, a total of 9 microchannel designs were considered, all with trapping sections 5 µm wide at their narrowest point. In all figures with microchannels the flow direction is from left to right.

3.1. Narrow microchannels

Microchannel design 1, designated as narrow microchannel, has a constant width of 100 µm throughout the 10 mm distance between the single inlet and outlet sections, with the trapping array section at the middle point of the microchannel (Figure 7). These microchannels present a simple trapping array design and therefore there is no need to widen that area, in this way also simplifying its microfabrication by dismissing the need of supporting structures. Furthermore, the narrow design contributed to the accumulation of cells in a smaller area, allowing a significantly easier observation of trapped cells when compared to the widened design. Two distinct trapping array solutions are used in narrow microchannels: 1a and 1b (elongated pillar-based).

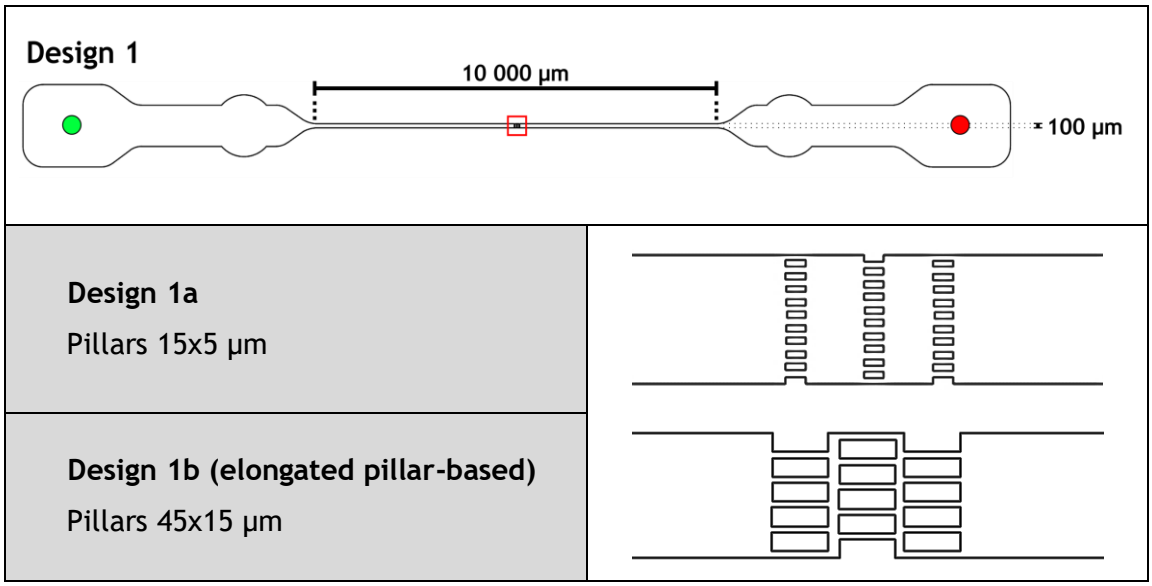

Figure 7 – Trap designs for the narrow microchannel

Flow direction from left to right. Green and red circles represent inlet and outlet points, respectively. Red square is the trapping array section, magnified bellow with the 2 different trap designs.

3.2. Widened microchannels

Since there is a higher possibility of clogging in the previously referred narrow microchannels, microchannel design 2 with a widened trapping array section is also considered. This design, designated as widened microchannel, has the same 10 mm distance between inlet and outlet sections and while most of the microchannel is 100 µm wide, the middle section width increases to 500 µm, where the trapping array section is located (Figure 8). This widened section allows introduction of more complex trapping array designs and larger pillars, being therefore less likely to suffer from clogging and bending issues[146]. However, widened microchannels require

introduction of supporting pillar structures (100x100 µm) as a way to prevent the widened section from collapsing. Three distinct trapping array solutions are used in widened microchannels: 2a, 2b (diamond pillar-based) and 2c (pyramid pillar-based).

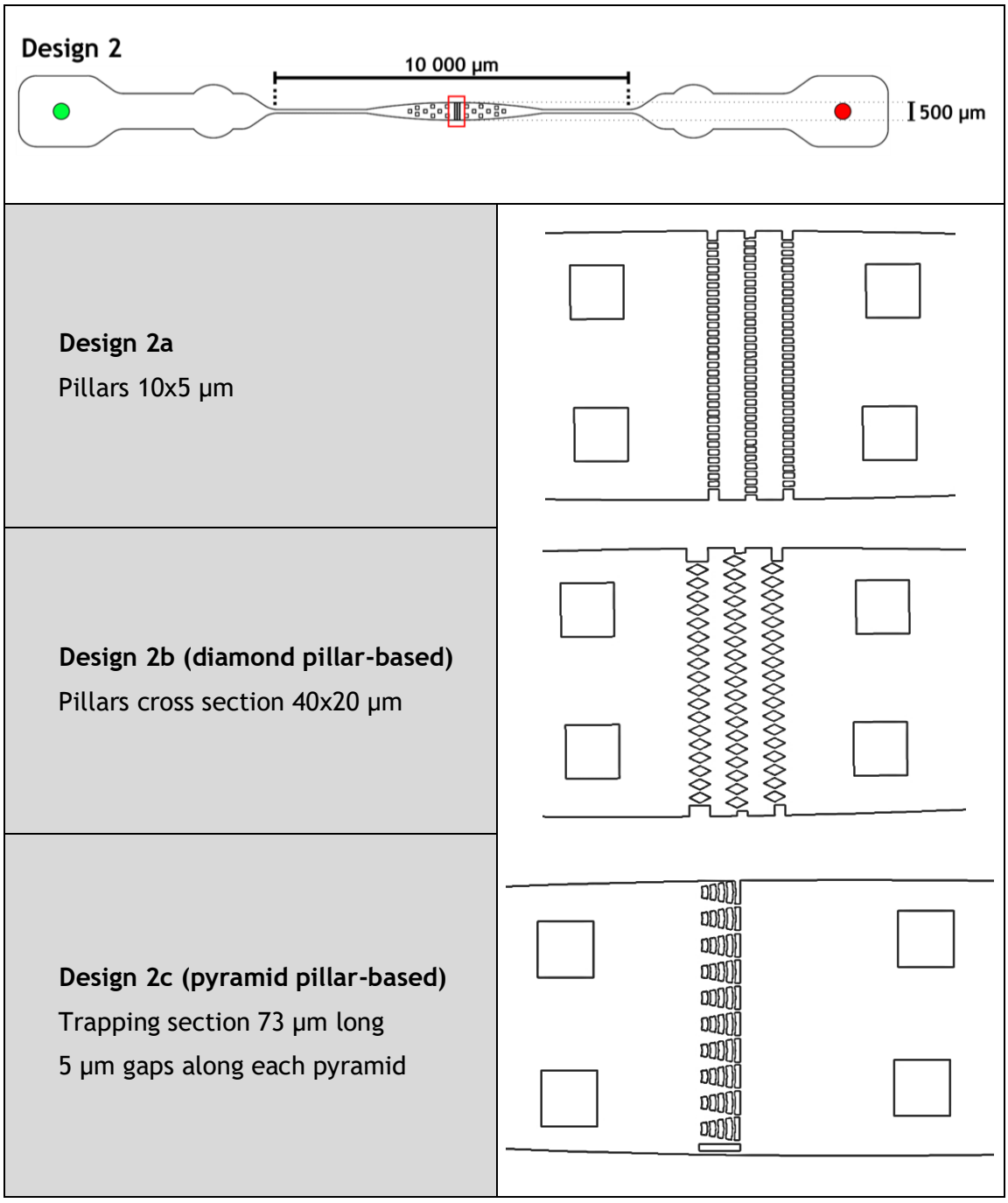

Figure 8 - Trap designs for the widened microchannels

Flow direction from left to right. Green and red circles represent inlet and outlet points, respectively. Red square is the trapping array section, magnified bellow with the three different trap designs.

3.3. Double inlet microchannels

With the intention of further reducing clogging occurrence, a set of double inlet microchannels were devised, one with three different pillar-based designs (Figure 9, microchannel design 3) and another with a single horse-shoe trap design (Figure 9, microchannel design 4). Since microfluidic systems work with laminar flows and therefore there is no discernable mixture of fluids in a stream flowing in contact[138], these designs intend to confine and/or redirect the cellular fluid through the addition of an auxiliary stream.

Design 3 resorts to a T-shaped microchannel with two inlets, one for cell suspension and one for control fluid (distilled water or an inert dye fluid, such as crystal violet, for visualization purposes). Such design is intended to allow redirection of the cell suspension to one side of the microchannel, if necessary.

Microchannel design 4 has a single inlet for cell suspension in the middle while a single inlet for the control fluid is divided into two streams and joins the cell suspension on each side of the microchannel, aiming to allow controlled restriction of cell suspension along the section of the microchannel that contains the single horse-shoe trap.

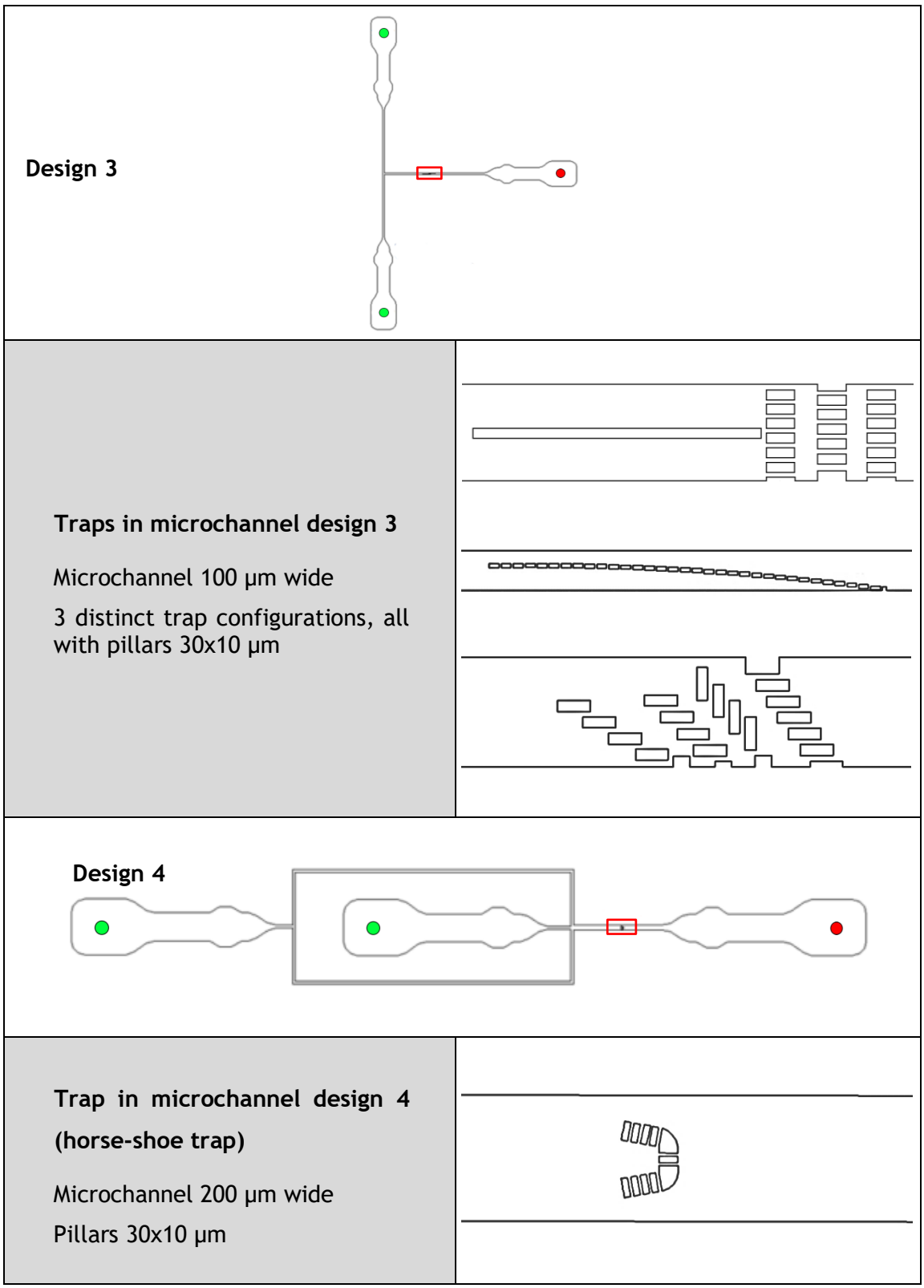

Figure 9 – Trap designs for the double inlet microchannels

Flow direction from left to right. Green and red circles represent inlet and outlet points, respectively. Red square is the trapping array sections, magnified bellow with the respective trap design.

4. Computational fluid dynamics simulations

Microchannel designs made in AutoCAD 2013 (Autodesk Inc., CA, USA) were gently provided by Moreira (2014)[15]. These designs were used as an input in Design Modeler 14.5.7 (Ansys, Inc., PA, USA) and discretized into a grid of quadrilateral cells by Meshing 14.5.7 (Ansys Inc., PA, USA). Finally, CFD simulations were run in Fluent 14.5.7 (Ansys Inc., PA, USA), allowing for a better understanding of behavior in the microchannels.

5. Microfabrication

For this project all geometries designed by Moreira (2014)[15] were considered, with three designs being selected for in-depth testing at the later stages of this project. A company specializing in microfluidics (microLIQUID, Mondragón, Spain) manufactured the SU-8 molds on a silicon wafer (master mold) by using chrome masks imprinted with the provided designs (photolithography technique). Each microchannel mold was produced in two depths, 30 and 50 µm (for the microchannel design 2b, diamond pillar-based, the 50 µm depth was not available during this project).

Microchannels were manufactured via the soft lithography technique. The master mold was placed in a closed environment with a few droplets of trichlorosilane (UCT Specialities, PA, USA) for 1 hour, in this way being submitted to a vapor deposition that allows an easier removal of the elastomer block to be imprinted[147]. A two-part silicone elastomer kit (Sylgard 184, Dow Corning, MI, USA) was used to produce a liquid polymer in a 5:1 base polymer to curing agent ratio (for each portion of base polymer, a fifth part of curing agent was added). To guarantee full contact between the base polymer and the curing agent, the mixture was placed on a mixer (VV3 vortex mixer, VWR International, PA, USA) for 10 minutes. After that, the liquid polymer was submitted to a degas procedure (desiccator connected to a G588DX vacuum pump, IDEX Corporation, IL, USA) until all air bubbles were removed. After pouring the liquid polymer over the master mold (previously treated with trichlorosilane vapor), another degas procedure was applied until there were no air bubbles in the mixture or trapped between the master mold and the polymer. Curing of PDMS was carried out at 80°C for 20 minutes (BD 23 Incubator, Binder GmbH, Tuttlingen, Germany). Then, the PDMS block containing the imprinted microchannels was cut, removed from the mold and holes were made in the inlet and outlet

sections of each microchannel with a precision tip 0.87 mm wide (20 gauge, Nordson EFD, OH, USA) for small holes and with an insulated end sleeve 2.5 mm wide (Cembre S.p.A., Brescia, Italy) for wider holes. Worth noting, the holes were punched on the imprinted side of the PDMS block, pushing the resulting residue to the non-imprinted side, thus preventing these residues from appearing inside the microchannel and possibly blocking fluid flow. To create a PDMS-PDMS seal, a glass slide was coated with PDMS (10:1 base polymer to curing agent ratio) using a spin coater (WS-650S, Laurell Technologies Corporation, PA, USA) at 5000 revolutions per minute for 50 seconds, creating a thin elastomer layer over the glass that would then be precured at 80°C for 15 minutes. After placing the 5:1 PDMS block on top of the 10:1 PDMS coated glass slide (with the imprinted microchannels facing the glass) and ensuring that no air bubbles nor other particles were interfering with the microchannels, the resulting chip was cured at 80°C for at least 12 hours.

5.1. Oxygen plasma treatment

As the hydrophilic effect acquired by exposing the PDMS to oxygen plasma treatment is lost overtime[127], the treatment was always applied immediately before introducing fluids into the microchannels, using a plasma cleaner system (ZEPTO model 2, Diener electronic GmbH, Ebhausen, Germany). In LOCs already constructed with PDMS-PDMS seal, the oxygen plasma treatment was applied with a power input of 30 watts through a microvacuum environment of 0.4 mbar for 2 minutes. To add hydrophilic properties to other equipment, such as syringes and Tygon tubing, a power input of 20 watts was applied through a microvacuum environment of 1.2 mbar for 30 seconds.

5.2. PDMS-glass seal

As an alternative to the PDMS-PDMS seal, the PDMS-glass seal was created by exposing both the imprinted surface of the PDMS block and a clean glass slide to oxygen plasma treatment (20 watts and 1.2 mbar for 30 seconds) and immediately joining the two surfaces. After 5 minutes the bond was secure.

As this step also comprises the addition of hydrophilic capabilities to the surface of the microchip, this method was executed immediately before introducing fluids into the microchannels. As such, after removing the cured PDMS block from the master mold, the PDMS was stored in a closed plastic petri dish with the imprinted surface facing up, not in contact with any surface and protected from dust. Also,

before receiving the oxygen plasma treatment, the glass slide was cleaned with ketone in a ultrasonic cleaner (VTUSC3. Velleman, Gavere, Belgium) for 8 minutes.

6. Contact angle measurements

Contact angle measurements were carried out using the sessile drop method, allowing determining the acquired hydrophilic capability of PDMS after the oxygen plasma treatment as well as loss of that effect overtime. For that, sections of 5:1 PDMS were submitted to oxygen plasma treatment (20 watts and 1.2 mbar for 30 seconds) and the mean value of the contact angle from 5 droplets (5 µl each) of ultrapure water (polar liquid with well-known surface tension components[148]) was assessed immediately at room temperature. Subsequently, the mean value of the contact angle of 5 droplets was also determined each 15 minutes for the next 2 hours. Also, for each test a non-treated 5:1 PDMS sample was used as control, measuring the contact angle of ultrapure water with the same volume and frequency (mean value of 5 µl droplets, placed each 15 minutes for a total time of 2 hours). Contact angles were determined using an OCA 15 Plus video-based optical measurement instrument with SCA 20 software (DataPhysics Instruments, Filderstadt, Germany).

7. Liquid handling strategies

In the regular system for introducing fluid into the microchannel, a 250 µl syringe (Hamilton Company, Bonaduz, Switzerland) connected to a Tygon tube (0.44 mm of internal diameter) was filled with at least 20 µl of the fluid to be introduced into the microchannel. A precision tip with 0.77 mm in diameter (21 gauge, Nordson EFD, OH, USA) was used to connect the tube to the inlet hole of the microchannel. The syringe was set on a neMESYS low pressure syringe pump (Cetoni GmbH, Korbussen, Germany) from which it was possible to control the flow rate of the fluid being introduced into the microchannel. Also, a precision tip with 0.77 mm in diameter was used to connect the outlet hole to another small Tygon tube, used as an exit of excess fluid.

Alternatively to this method, a reverse flow system was devised during this project, where the same syringe/tubing apparatus was placed in the syringe pump and a negative value for flow rate was used (pulling fluid from the microchannel). The connection of the apparatus to the microchannel was obtained via the same

precision tip to the outlet hole of the microchannel. At least 5 µl of fluid was introduced directly into a widened inlet hole (made with an insulated end sleeve 2.5 mm in diameter) with a pipette (Eppendorf, Hamburg, Germany).

The capillary effect caused by the hydrophilic properties added to microchannels by oxygen plasma treatment is also considered to be a liquid handling strategy when fluid is first introduced into an empty microchannel, although being a passive strategy because it does not allow control over flow velocity[126, 149]. This liquid handling strategy is particularly relevant in the reverse flow system: whereas the regular system still requires activation of the neMESYS low pressure syringe pump to introduce fluid into the microchannel for the first time, in the reverse flow system the fluid is placed in direct contact with the inlet hole, at which point the capillary effect immediately comes into play and the fluid fills the microchannel.

8. Microchannel retention tests

To assess the ability of the microchannels to entrap cells, 10 µl of a solution with 10^3 cells/µl of previously fixed and permeabilized *S. cerevisiae* cells suspended in ethanol was introduced into the microchannels via the widened inlet well, while the syringe array was connected to the outlet of the microchannel (reverse flow system). The flow rate set to pull the fluid on the neMESYS pump was 1 µl/minute, as a higher flow rate could remove individual cells from the trapping sections, and the trapping array section was recorder with an inverted microscope (subchapter III - 10).

The obtained videos were then used to count the number of cells flowing through the trapping arrays versus the number of cells being retained during the first minute (starting as soon as the fluid passed the trapping arrays). This was performed using VLC media player 1.1 (open source software) set at 0.5x playing speed and with the motion detection tool turned on.

9. PNA-FISH in microchannels

The PNA-FISH protocol inside a microfluidic environment was performed with the reverse flow system. As such, 10 µl of a previously fixed cell suspension (10^4 cells/µl) was introduced into the widened inlet hole of oxygen plasma treated microchannel with a pipette (Eppendorf, Hamburg, Germany). Since fluid entered the microchannel due to capillarity effect, no action from the syringe pump was necessary at this stage. After 10 minutes, the excess fluid in the inlet hole was

removed with absorbent paper and 10 µl of the hybridization solution was added to the inlet hole. From this moment on, the LOC was protected from light with aluminum foil sheets as to not degrade the fluorescent label of the probe. Using the neMESYS syringe pump, the hybridization solution was pulled through the microchannel at the established rate of 1 µl/minute for 5 minutes. The pump was then stopped, the inlet hole was covered with 18x18 mm cover slips (Menzel Gläser, Braunschweig, Germany) and the apparatus was disconnected from the pump (while maintaining tubing and syringe connected to the exit hole) and incubated at 54 or 59 ºC (the optimal hybridization temperature depending on which probe was used) for 1 hour in the drying and heating chamber. Afterwards, the apparatus was again connected to the syringe pump, hybridization solution in excess was removed from the inlet hole with absorbent paper and 10 µl of washing solution (pre-heated in the incubator at 54 or 59 ºC, depending on the probe used) was added, while the syringe pump was pulling at the established rate of 1 µl/minute for a total of 5 minutes. Once more, the pump was stopped, the inlet hole was closed with a cover slip, and the entire apparatus was disconnected from the pump and incubated at 54 or 59 ºC for 30 minutes. Finally, the washing solution in excess was removed from the inlet hole and 10 µl of distilled water was added to the inlet hole and pulled through the microchannel for 10 minutes at a rate of 1 µl/minute. After this, presence of fluorescent signal inside the microchannel could be observed in an inverted epifluorescence microscope (subchapter III - 10). A schematic representation of this procedure is presented in Figure 10.

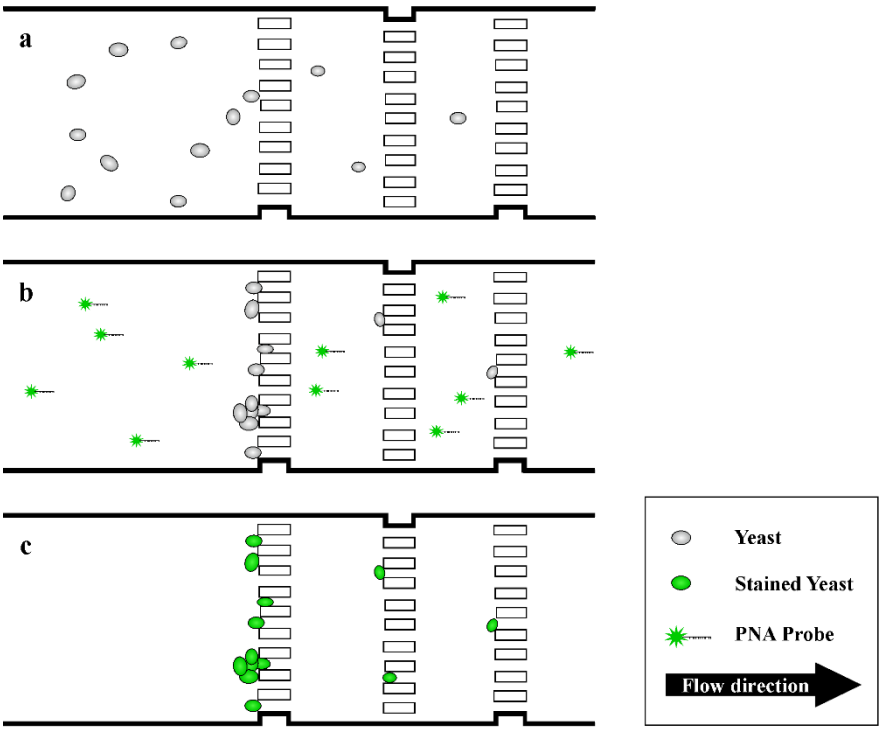

Figure 10 – Schematic illustration of the concept to perform FISH assay in microchannels

(a) Yeast cells flowing through the microchannel are trapped at the 5 µm gaps created by the pillars at the trapping array section; (b) The PNA probe solution is pulled through the device at a constant flow rate, hybridizing with the retained yeast cells; (c) After hybridization, washing solution is introduced into the microchannel to remove loosely bound and excess probes. The washing solution is then replaced by distilled water and examining the trapping array section with an epifluorescence microscope will reveal the fluorescently-labeled yeast cells. Adapted from Moreira (2014)[15].

10. Microscopic visualization

Visualization of fluorescent signal in glass slides was performed with a Leica DM LB2 epifluorescence microscope, equipped with a Leica DFC300 FX camera controlled via the software Leica Application Suite 4.2.0 (Leica Microsystems, Wetzlar, Germany).

To access movement inside microchannels during the introduction of fluids, a Leica DMI 5000 inverted microscope was used, allowing to capture still images and videos with a Leica DFC350 FX camera controlled by the software Leica Application Suite 3.7.0 (Leica Microsystems, Wetzlar, Germany).

Fluorescent signal inside the microchannels was visualized with an inverted epifluorescence microscope Nikon Eclipse Ti-E connected to a DS-Ri2 camera and imaging software NIS-elements 4.13.04 (Nikon Instruments, Amsterdam, Netherlands). The microscope was equipped with a FITC (fluorescein isothiocyanate) filter sensitive to the fluorophore Alexa Fluor 488 attached to the PNA probe

(excitation 465 to 495 nm, barrier 515 to 555 nm, dichroic mirror 505 nm) and to confirm absence of cell autofluorescence a G-2A (green excitation longpass) filter was used as negative control (excitation 510 to 560 nm, barrier 590 nm, dichroic mirror 575 nm). When using the fluorophore Alexa Fluor 594, the microscope was equipped with a Live/Dead filter (excitation 530 to 550 nm, barrier 570 nm, dichroic mirror 591 nm).

To guarantee consistency in the obtained results, software parameters of all microscopes (exposure, gain and saturation) were maintained constant throughout the experiments involving PNA-FISH.

IV. Results and discussion

1. Adaptation of PNA-FISH protocol to microfluidic environment
2. Selection of microchannel and trapping array designs
3. Surface hydrophilicity obtained by oxygen plasma treatment
4. Introduction of cells into microchannels
5. Influence of focus plane on cell detection
6. Cell retention efficiency
7. PNA-FISH in microfluidic environment

1. Adaptation of PNA-FISH protocol to microfluidic environment

While this project intends to include the entire PNA-FISH procedure in a microfluidic environment, it must be noted that the protocol of PNA-FISH is quite complex, with several variables that can impact the resulting detection efficiency[150]. As such, during this initial stage of the project more significance was attributed to the three following factors: cell retention in the trapping array section, hybridization of PNA probes in a scaled-down environment and signal detection inside the microchannel. As a way to reduce variables, the fixation/permeabilization step with paraformaldehyde 4% (w/v) and ethanol 50% (v/v) was performed outside the microfluidic environment. Therefore, cells introduced into the microchannels were suspended in ethanol 50% (v/v) and tests were performed to verify both entrapment and hybridization efficiencies, as well as determining if florescent signal detection inside the microchannel possible.

Also, after executing cell growth protocol and its fixation/permeabilization, cells can be stored at -20°C for up to 6 months, during which time cells could be promptly used in microfluidics experiments. This allows surpassing the need to grow a new cellular culture before each microfluidic experiment, thus dismissing the repetition of cellular growth in culture media broth overnight and then again in a new culture media for at least 4 hours.

To assess if using previously fixed/permeabilized cells would affect the retention capabilities of microchannels when compared to non-fixed cells, both were introduced into microchannels at the original concentration of 10^4 cells/µl and retention efficiency was compared. Non-fixed cells diluted in PBS presented a higher resistance in flowing through the trap section than that observed by using fixed cells diluted in ethanol. Consequently, the risk of air bubble formation was increased when using non-fixed cells diluted in PBS. Also worth noting, a higher amount of cells flowing through the microchannel was observed when non-fixed cells where used, being possible to reduce the minimal cellular concentration necessary for efficient detection. Although this increase in cell number can be attributed to the denser nature of the PBS when compared to ethanol[151, 152], which can lead to reduced settling of cells along the Tygon tube when using PBS, it is more likely that the higher number of cells observed in non-fixed state is due to the fact that they were only submitted to one centrifugation process (to transfer cells from growth medium to PBS), whereas in the fixation/permeabilization protocol they are submitted to two

centrifugations (cells are transferred from growth medium to paraformaldehyde and then to ethanol), therefore increasing the possibility of losing cells in the discarded supernatant.

Although the permeabilization protocol compromises the cell membrane structure[49], fixation prevents variation in cell size. As such, cells submitted to the fixation/permeabilization protocol have shown similar size to that of non-fixed cells, meaning that no change in the retention efficiency of microchannels should occur when using fixed cells compared to that achieved with non-fixed cells.

1.1. Probe optimization

The PNA probe targeting *S. cerevisiae* 26S rRNA initially used in this project was designed by Meireles (2012)[143] and connected to an Alexa Fluor 594 dye, presenting red fluorescence. However, by performing the PNA-FISH procedure both in suspension and slides, it was clear that the fluorescent signal was weaker than expected, usually insufficient to be captured by the camera connected to the microscope (Figure 11 a). These poor results may be attributed the fact that this probe was synthetized in 2012 and the Alexa Fluor might have since gradually lost its fluorescent capabilities by accumulated exposure to light.

Since it is intended to observe the target cells inside a microfluidic environment, it is expected that the added visual barriers of glass and/or PDMS could contribute to diminish the fluorescent signal. As such, a new PNA probe was utilized. As there was no need for a specific probe to *S. cerevisiae* at this stage of the project (since no other type of cells were being introduced into the microchannels), the new PNA probe was the same as used in other projects in the laboratory. This probe targets rRNA from Bacteria, Archaea and Eukarya cells and is connected to an Alexa Fluor 488 dye, presenting green fluorescence.

As stated in Chapter III (Material and methods), thermal stability is related to probe affinity to the target[145]. However, the calculations that determine theoretical melting temperatures usually overestimate the ideal hybridization temperatures to be used, as they fail to take into consideration several parameters in the hybridization solution (such as denaturants) that can reduce the melting temperature of double-stranded nucleic acids[153, 154]. As such, a trial and error procedure was devised, where the FISH procedure in slides was performed with different hybridization temperatures: 51, 53, 55, 57 and 59 ºC.

As no denaturants such as formamide are used in the hybridization solution, the higher temperature of 59 ºC, closer to the theoretical melting temperature of 62.4 ºC, was tested first. Hybridization of the probe at 59 ºC effectively marked the *S. cerevisiae* cells with a strong green fluorescent signal (Figure 11 b). A lower temperature of 57 ºC was also tested, resulting in a slightly diminished fluorescence when compared to the 59 ºC temperature. Consequently, the optimal hybridization temperature for the new PNA probe was set at 59 ºC.

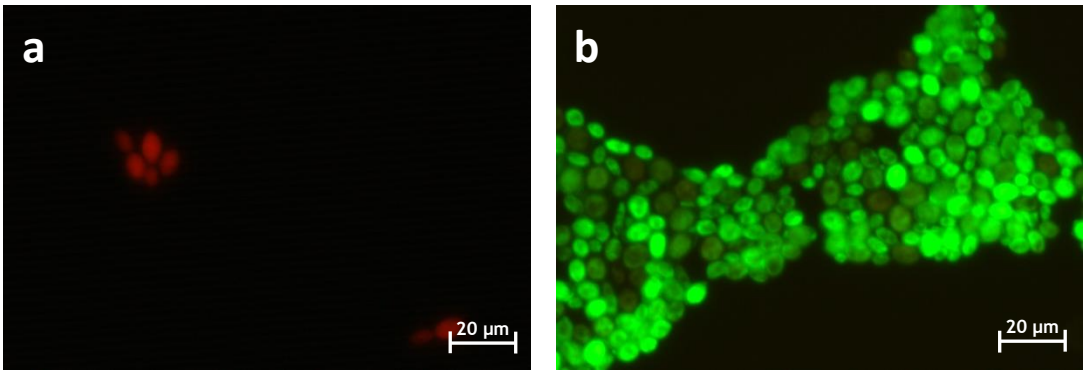

Figure 11 - Fluorescent signal presented in *S. cerevisiae* cells marked with different PNA probes
(a) The PNA probe targeting *S. cerevisiae* 26S rRNA (hybridization temperature of 54 ºC) presented a poor red fluorescent signal; (b) The new PNA probe, capable of targeting rRNA from Bacteria, Archaea and Eukarya cells (hybridization temperature of 59 ºC) was capable of marking all *S. cerevisiae* cells with a strong green florescent signal. Original magnification 1000x.

2. Selection of microchannel and trapping array designs

Considering the microchannel designs provided by Moreira (2014)[15] from which molds were already fabricated by photolithography, it was necessary to select those that had higher cell retention efficiency, which could then be submitted to further testing. Retention ability is dependent on a reliable microfabrication procedure, allowing to obtain LOCs with no construction errors such as bending issues. Bending issues arise when the stability of microstructures made of a soft material (as is the case with PDMS) is compromised, usually because the height of the structures imprinted onto the elastomer surface is too high compared to the separation between them, resulting in the collapse of pillar structures (ground collapse) or even collapse of the unpatterned spaces (roof collapse)[155].

First considering the narrow microchannel configuration (Figure 7), the design 1a showed significant problems as it was very difficult to reproduce via soft lithography. This was due to the trapping array pillars lack of structural support, being just 15 µm

long and 5 µm wide, which resulted in frequent bending issues. Consequently, there was an occurrence of wide gaps through which cells were able to escape, severely affecting the retention capability of this design. Still, while ground collapse was often observed in microchannels, roof collapse was never an occurrence. On the contrary, bending issues were seldom observed in design 1b (elongated pillar-based design) due to the increased support capabilities of the pillars: while the height used for this comparison was the same in both designs (30 µm), each pillar of the design 1b is larger, 45 µm long and 15 µm wide. As such, the design 1b was the only narrow microchannel considered for subsequent testing.

Regarding the widened microchannel configuration (Figure 8), the trapping array design 2a was proven to be problematic during microfabrication due to lack of support provided by the pillars: since it has the same sized pillars as the design 1a (15x5 µm), the previously described problem persists and the pillars usually collapse, creating wide gaps in between. Again, no roof collapse was observed, possibly due to the 100x100 µm supporting pillar structures added to widened microchannels. The remaining trapping array designs, 2b (diamond pillar-based design) and 2c (pyramid pillar-based design), are constituted by stable pillars and rarely presented bending issues, therefore being both considered for further testing. A comparison between occurrence of bending issues in widened microchannels is presented in Appendix IV - Figure 27[15].

Finally, it was possible to observe that fluid flow inside double inlet microchannels (Figure 9) can be controlled as intended by Moreira (2014)[15]. By varying the two inlet flow rates, one containing the cell suspension (represented by a dye fluid, crystal violet) and the other containing an inert fluid (distilled water), the cell suspension can be redirected to a single area of trapping arrays in design 3, allowing to diminish the risk of clogging (Figure 12 a), or the cell suspension can be restricted to the middle section of the microchannel design 4, which is essential for the success of a single horse-shoe trap design (Figure 12 b). However, since these double inlet microchannels require a careful control of two distinct fluid flows in pair with constant observation of the trapping array section as way to decide whether an alteration in the cellular fluid flow is necessary, the complexity of the procedure is increased. As in this early stage of the project it is intended to keep the microfluidic device as simple to use as possible, the double inlet microchannels were not considered for further testing.

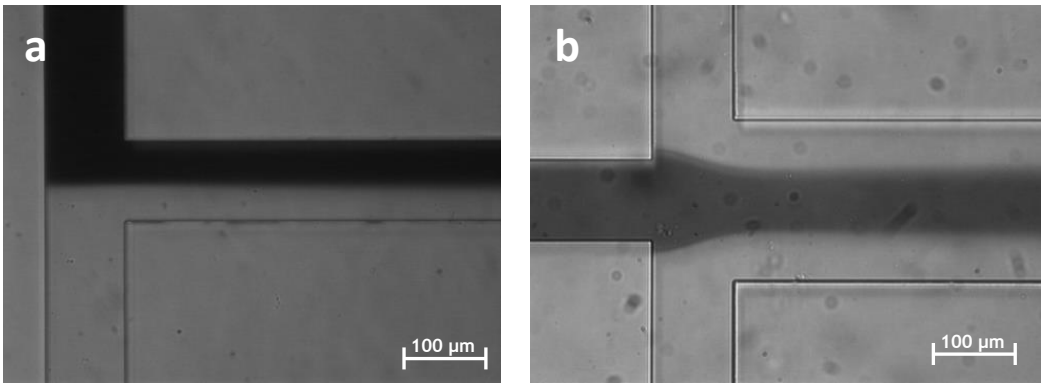

Figure 12 - Tests with water and crystal violet in double inlet microchannels

(a) Design 3 allows restriction of fluid flow to a single side of the microchannel; (b) Design 4 allows constriction of fluid flow to the middle section of the microchannel. Original magnification 200x.

Summarizing, the microchannel designs considered for subsequent tests were:

- 1b – Narrow microchannel with elongated pillar-based traps (Figure 7);
- 2b - Widened microchannel with diamond pillar-based traps (Figure 8);
- 2c - Widened microchannel with pyramid pillar-based traps (Figure 8).

2.1. Microchannel depth

Besides pillar size and shape, pillar height affects tendency to bending issues, with higher pillars often leading to the appearance of gaps in the trapping array through which cells can easily pass without any hindrance[100]. For this reason, it was necessary to access which of the available master mold depths, 30 or 50 µm, was capable of producing microchannels with fewer microfabrication errors. Also worth noting, while for designs 1b (elongated pillar-based) and 2c (pyramid pillar-based) both depths were available and compared, only the 30 µm depth master mold was available for the design 2b (diamond pillar-based).

During microfabrication procedure it was possible to observe that bending issues were significantly more frequent and severe in microchannels with a depth of 50 µm, where narrow pillars would be taller and therefore more lacking in support (Figure 13 a). Meanwhile, the resulting microchannels created through soft lithography with 30 µm master molds constantly presented less construction flaws due to pillars toppling over or bending (ground collapse), being possible to obtain perfectly constructed microchannels more often (Figure 13 b). The same occurrence was also generally observed in the pyramid pillar-based design.

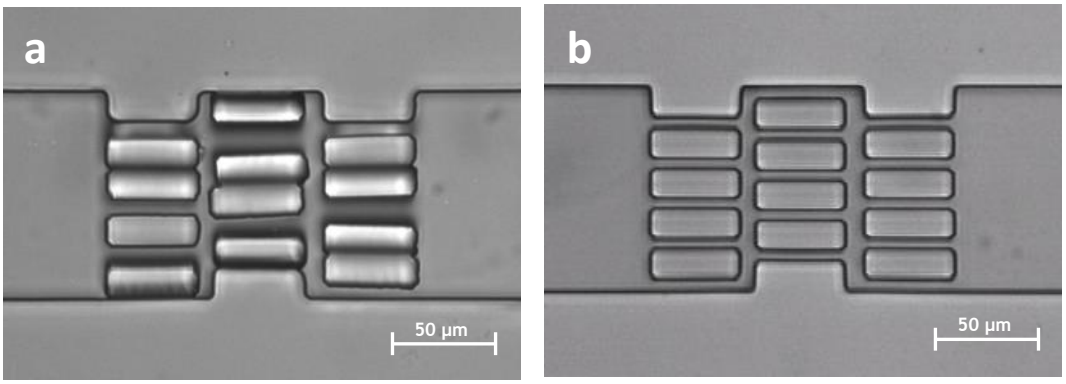

Figure 13 - Microfabrication errors in different microchannel depths

(a) Elongated pillar-based design with 50 µm depth presented toppled over pillars more often than (b) the same design with 30 µm depth. Original magnification 400x.

Considering these aspects, microchannels with 30 µm depth were selected as ideal for the following tests. Still, microchannels with 50 µm depth were also used when construction issues were inexistent or at least not severe, in this way obtaining more results capable of further highlighting the differences between microchannel configurations.

2.2. Computational fluid dynamics simulations

All microchannel designs were tested by Moreira (2014)[15] in computational fluid dynamics (CFD) simulations before fabricating the SU-8 master molds, allowing visualization of fluid flow and its velocity. To better understand upcoming results, CFD simulations of the three selected trapping array designs (elongated pillar-based design in a narrow microchannel, diamond and pyramid pillar-based designs in widened microchannels) were again performed and included in this project.

In the CFD simulation results presented in Figures 14 and 15 it is visible that fluid velocity increases from the wall to the center of the microchannel (as expected from the illustration in Figure 3). Higher flow velocity profiles are observed in the trap array section of the narrow microchannel with elongated pillars, especially along the longitudinal sections with 5 µm width (Figure 14). However, the offset distribution of the three rows of pillars generates a section between them where flow velocity is slowed down.

CFD simulations of the trap array section on the selected widened microchannels, diamond and pyramid pillar-based, show an overall lower fluid velocity when compared to that observed in the narrow microchannel, with a magnitude of velocity around ten times smaller (Figure 15). It is also evident that the 100x100 µm supporting pillars do not affect regular flow in the trapping array section

of the microchannel. Noteworthy, the narrow spaces between traps of the pyramid pillar-based design (Figure 15 b) are longer than those in the diamond pillar-based design (Figure 15 a) and so the flow velocity in that area is significantly increased. Also, the repetition of pillar rows in the diamond pillar-based design creates two areas between these rows where fluid flow velocity is reduced.

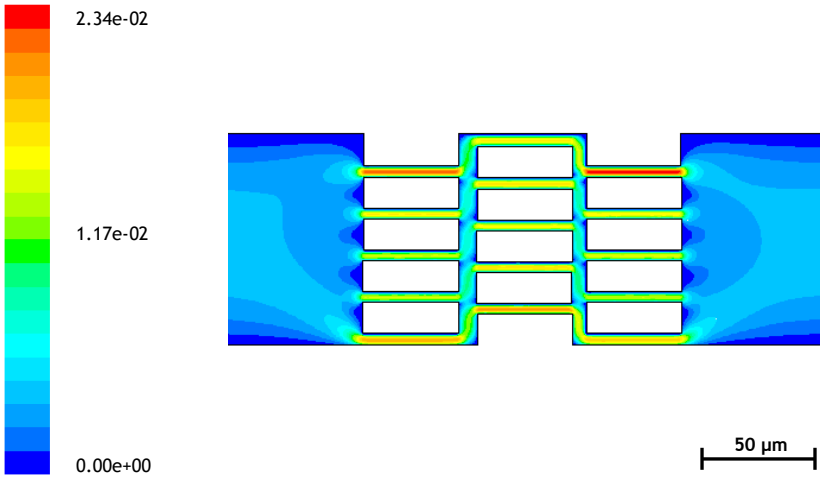

Figure 14 – CFD simulation in the trapping array section of a narrow microchannel

The design 1b (elongated pillar-based) is used for the simulation along the horizontal plane of symmetry. Color scale represents the contours of velocity magnitude (m/s).

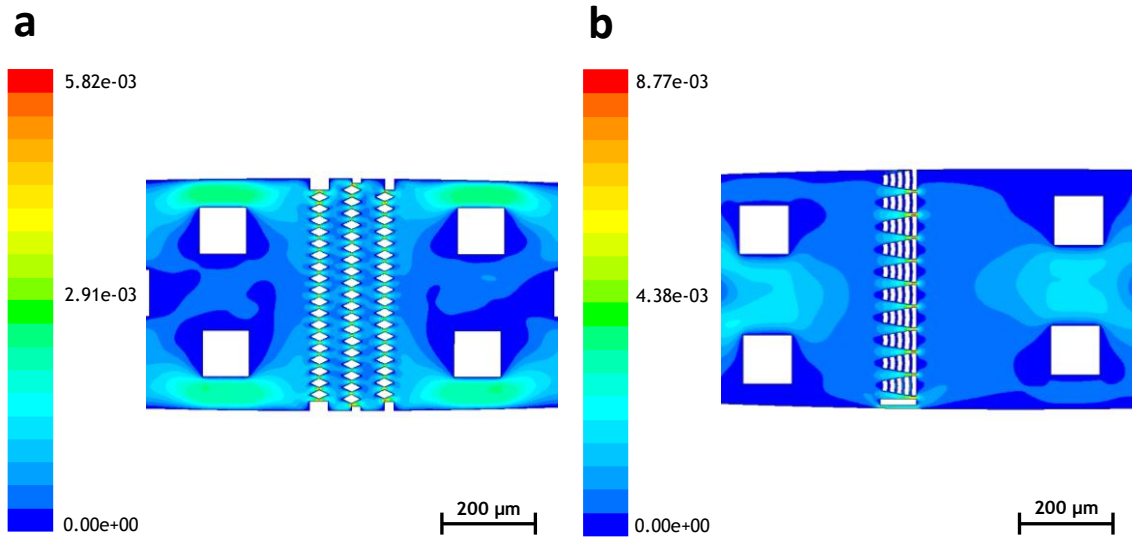

Figure 15 – CFD simulation in the trapping array section of widened microchannels

(a) Design 2b (diamond pillar-based); (b) Design 2c (pyramid pillar-based). Simulations done along the horizontal plane of symmetry of the microchannels. Color scale represents the contours of velocity magnitude (m/s).

CFD simulations and flow lines performed during this project for all narrow and widened microchannel designs are presented in Appendix V – Figure 28.

3. Surface hydrophilicity obtained by oxygen plasma treatment

When introducing polar solvents into microchannels, air bubble formation may disrupt the expected liquid flow demonstrated by CFD simulations, thus decreasing the expected trapping efficiency. In fact, preceding works evidenced that air bubbles inside the microchannels pose as one of the main problems for this novel procedure, since small air bubbles were often found in the trapping array section of the microchannel disrupting retention capabilities or, in more severe cases, large air bubbles were able to completely block the microchannel[15].

As mentioned in the Chapter II (Literature review), formation of air bubbles inside microchannels is a direct consequence of the hidrophobic nature of PDMS[125]: the surface of the microchannel will repel the introduced fluid, leading to air bubble accumulation mainly in sections with high contact surface area, as is the case with the trapping array section. The answer for this challenge may rely on oxygen plasma treatment: by submitting PDMS to a partially ionized gas, polar functional groups (mainly silanol groups) are added to its surface, in this way generating a temporary hydrophilic state[124].

However, overexposure to oxygen plasma treatment on polymeric PDMS blocks may lead to formation of surface cracks and even detachment from the glass[127], which has an added significance given the fact that the PDMS base/curing agent used throughout this project has a ratio of 5:1 and, therefore, the resulting PDMS block is harder and more susceptible to cracks than PDMS blocks constructed with the most commonly used PDMS base/curing agent ratio of 10:1[117]. The larger ratio of curing agent used in this project allowed to attain a viscous PDMS mixture, guaranteeing that PDMS is able to acquire all the details from the master mold when poured over it. Still, after the curing process, a relatively soft and ductile PDMS block is obtained, which allowed removal from the mold without damaging the imprinted structures.

As such, to ensure that PDMS structure was not affected by cracks, oxygen plasma treatment was applied for a short period of time. Such short exposure to the treatment might lead to a reduced duration of the intended effects and thus the variation in hydrophilic capabilities of oxygen plasma treated PDMS surfaces was assessed overtime in the following set of experiments.

Effects of the oxygen plasma treatment on the hydrophobic nature of PDMS surface are evidenced in Figure 16. When first filling up non-treated microchannels

with cell suspension, besides being very difficult to remove all air bubbles (a relatively high flow rate, at least 10 µl/minute, was usually necessary), the initial hindrance in fluid flow due to the hydrophobic nature of the microchannel often resulted in some cells being left attached to the PDMS surface at the inlet section. Oxygen plasma treated microchannels have shown significantly better results, as air bubbles were easily removed even at minimal flow rates (1 µl/minute) and a negligible amount of cells was found in the microchannel area preceding the trapping arrays.

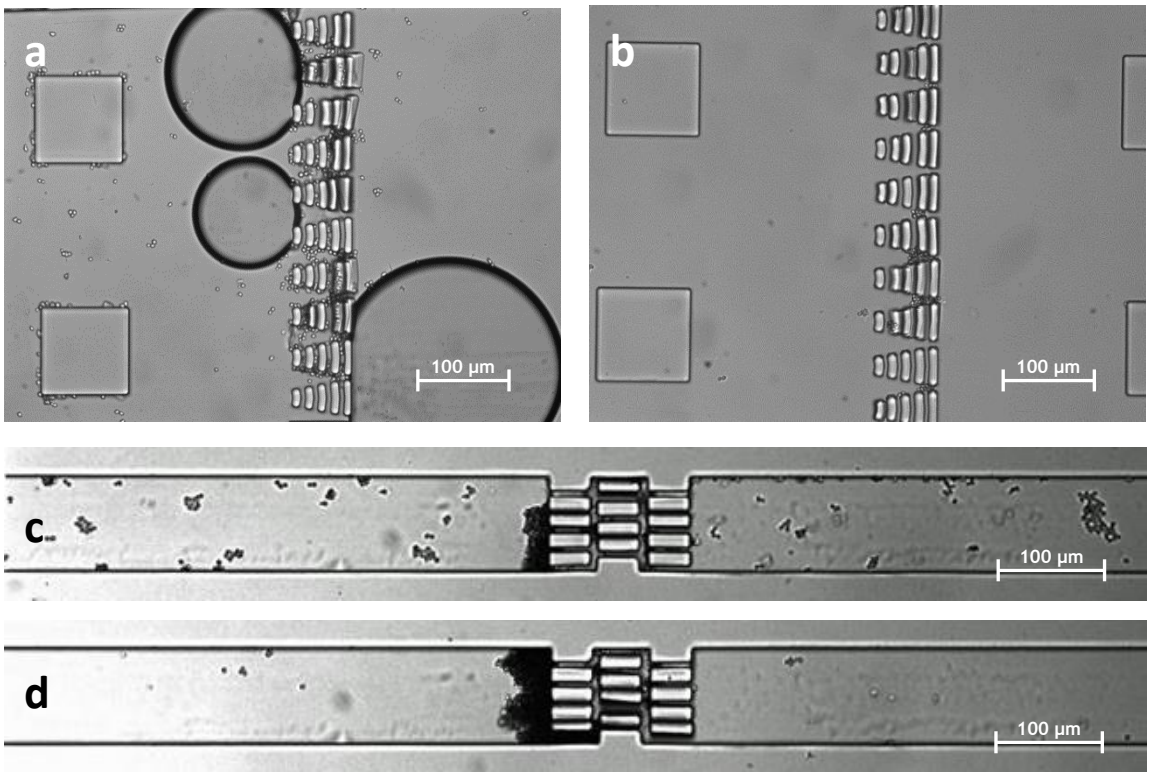

Figure 16 – Comparison between non-treated and oxygen plasma treated microchannels

The effect of oxygen plasma treatment is evident in pyramid pillar-based design non-treated (a) and treated (b), as well as elongated pillar-based design non-treated (c) and treated (d). Oxygen plasma treatment reduces air bubble formation inside microchannels (visible by comparing a to b) and, since fluid flow is constant, more cells are able to reach the trapping array section (visible by comparing c to d). Cell concentration of 10^4 cells/µl. Original magnification 200x.

Worth mentioning, the amount of cells observed after the trapping array section in Figure 16 a and c is explained by the higher fluid flow necessary to clear the air bubbles from the traps, which results in cells being dragged through the narrow spaces between pillars, an effect explained in detail in the upcoming subchapter IV – 4.1.

3.1. Contact angle tests

To determine the hydrophilic capabilities added to the PDMS surface by oxygen plasma treatment, as well as the decline of these effects over time, the sessile drop contact angle method was applied. Figure 17 presents the mean values of 8 repetitions of contact angle measurements of ultrapure water in oxygen plasma treated PDMS (as described in Chapter III - Materials and methods), along with the mean value of contact angles of ultrapure water in untreated PDMS. As previously mentioned during Chapter II (Literature review), the surface is regarded as hydrophilic if an angle of contact lower than 90 degrees occurs, whereas if the angle of contact is higher than 90 degrees the surface is considered to be hydrophobic[137].

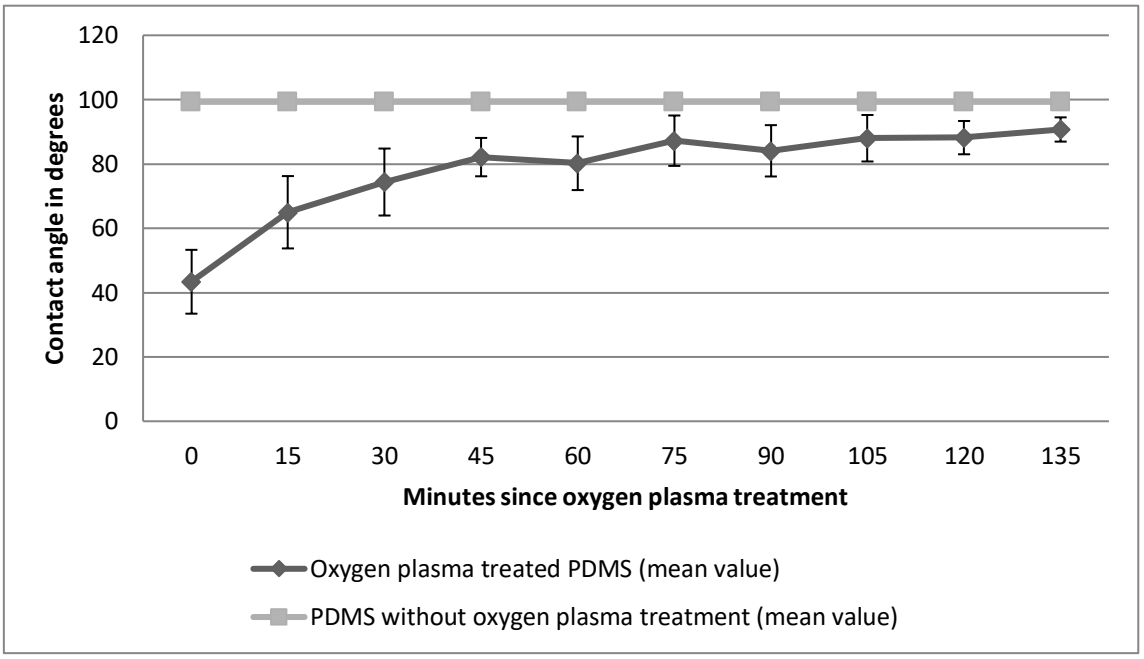

Figure 17 – Mean values of distilled water contact angle with both non-treated and oxygen plasma treated PDMS along time

Error bars represent standard deviation. Lower contact angles are obtained for 1 hour after the oxygen plasma treatment occurs and, as such, this is the ideal time window to perform microfluidics experiments. The hydrophilic properties acquired by the treated PDMS can be verified for up to 2 hours after treatment.

Throughout these measurements it was possible to assess that oxygen plasma treated PDMS is able to retain hydrophilic capabilities for approximately 2 hours, after which time the contact angle reaches 90 degrees and the PDMS properties acquired by oxygen plasma treatment become negligible. The lower contact angle results were observed during the first hour and, as such, the first hour after oxygen plasma treatment was considered to be the optimal time window to introduce cell fluid into the microchannels in the subsequent experiments. Still, it is worth

mentioning that even after 24 hours the contact angle of oxygen plasma treated PDMS did not reach the value observed in non-treated PDMS (approximately 100 degrees).

These same conclusions were validated by microfluidics experiments, where during the first hour after treatment no hindrance in fluid movement was observed in the trapping array section and air bubbles were removed almost instantaneously, although it was often possible to fully remove all air bubbles by introducing the fluid even 2 hours after the oxygen plasma treatment.

Still, as already mentioned in Chapter II (Literature review), storing oxygen plasma treated PDMS in vacuum, low temperatures and/or in water prevents the reorganization of the silanol group[127], which can ultimately extend the obtained hydrophilic properties beyond the accessed 1 hour.

3.2. PDMS-glass seal

Up until this point, the microfabrication process relied on a PDMS-PDMS seal, which comprised the adhesion of a 5:1 PDMS block with the imprinted microchannels to a glass slide covered in a thin layer of 10:1 PDMS. Then, to form a covalent bond between these two sections of the LOC, an additional curing process at 80°C for at least 12 hours was needed. Although the bonding strength between PDMS block and PDMS coated glass resulting from this process is able to withstand pressures up to 5 psi[105], thus being adequate for use with the intended flow rate of 1 µl/min, mishandling the microchip could easily cause detachment of the two sections[135].

An alternative method for the last step of microfabrication has since been implemented, in which the glass is not covered by a layer of PDMS but instead both the PDMS and glass surfaces are submitted to oxygen plasma treatment and, when joined, a covalent bond is formed, permanently attaching the PDMS to the glass and thus sealing the LOC system[134]. This PDMS-glass seal suppresses the need for an overnight curing step and already comprises the oxygen plasma treatment step, making the overall microfabrication process at least 12 hours faster. Also, the resulting bond created between the PDMS and the glass slide is much stronger than the previously obtained bond in such a way that the microchannel is capable of withstanding higher flow rates without risk of bursting[111, 134], being highly unlikely that the PDMS becomes detached from the glass during microchip handling or transportation[135].

As it was established in the previous subchapter that oxygen plasma treatment was beneficial for the fluid flow inside the microchannel, oxygen plasma treatment protocol was adapted to be used for PDMS-glass seal for all subsequent experiments, in this way making the microfabrication protocol more efficient.

4. Introduction of cells into microchannels

Upon introducing the cells into oxygen plasma treated microchannels with PDMS-glass seal, a series of problems were tackled sequentially, namely defining the ideal flow rate to guarantee cellular retention in the designed areas and selecting a cell concentration that allowed to visualize the efficiency of traps by counting the retained cells versus non-retained cells. Also, a complication where cells were being stuck in the tubing system was tackled by 2 different methods, oxygen plasma treated tubes and reverse flow system.

4.1. Flow rate

Flow rate inside the microchannels is an important aspect to be considered, particularly in the trapping array section. A higher flow rate results in a faster procedure, allowing analysis of a higher volume of the targeted sample in less time. However, increasing the flow rate implies that cells are more likely to flow through the traps and even previously trapped cells can be dragged away. This proposition is supported by CFD simulation results that have shown that fluid velocity is significantly higher in the narrowing section of the traps than any other section of the microchannel (Figures 14 and 15).

In order to select an appropriate flow rate, tests were conducted to visually assess cell retention capabilities of all three selected microchannel designs while altering the inlet fluid flow rate, using a suspension of fixed cells in ethanol at the concentration of 10^4 cells/µl. At 1 µl/minute, the lower flow rate tested, cell movement was fully visible throughout the microchannels under an inverted microscope. While some cells acquired considerable higher velocity in the narrow sections of the trapping arrays, most cells (especially those in agglomerates) were effectively retained in the trapping array section. After being trapped, usually no further movement was observed in these cells.

Increasing the flow rate to 5 µl/minute, the significantly higher velocity registered in the narrow sections meant that individual cells squeezed through the traps more often. However, these flow rates did not remove cells once they were

captured in the trapping array section. Also, counting the cells flowing through the traps (needed in following experiments as a way to assess retention rate) was increasingly difficult, although using a high-speed camera (not available for this project) could surpass this problem.

At flow rates of 10 µl/minute and above, a significantly higher number of cells (both in the individual form and in aggregates) could flow through the traps and their high velocity made retention rate assessment practically impossible. Furthermore, dragging of previously trapped cells was observed (Figure 18).

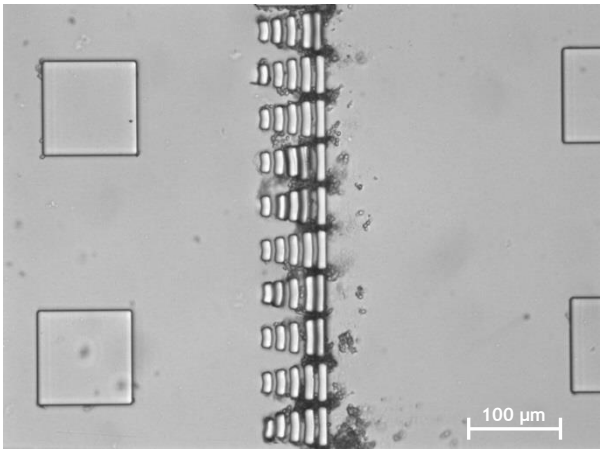

Figure 18 – Cells being removed from traps due to an excessive flow rate

For demonstration purposes, a flow rate of 20 µl/minute was applied in this case. This phenomenon often occurs with flow rates higher than 10 µl/minute. Original magnification of 200x.

To ensure that the highest possible number of cells was retained without dragging effect and that counting of all cells flowing through the traps was possible, the flow rate of 1 µl/minute was set as standard for following procedures.

4.2. Cell concentration

During initial assessment of retention capabilities of microchannels, a concentration of approximately 10^7 cells/ml (10^4 cells/µl) was used. It was however evident that cell concentration introduced into the syringe/tube system appeared to be lower when observed passing through the microchannels. While the number of cells flowing through the microchannel was sufficient to assess retention capabilities of traps, an effective $1x10^4$ cells/µl concentration should likely fill the trapping array section with cells, which was not observed.

This hypothesis was further supported by doing a simple dilution of the cell suspension in ethanol, from 10^4 cells/µl to 10^3 cells/µl, and introducing this new concentration into the microchannel. In this experiment, very few cells were

observed inside the microchannel at a flow rate of 1 µl/minute. As a proof of concept, the flow rate was increased to 5 µl/minute and even then the amount of cells to effectively assess retention capabilities were insufficient, meaning that the current cell concentration flowing through the microchannel is in fact significantly reduced from that introduced into the system.

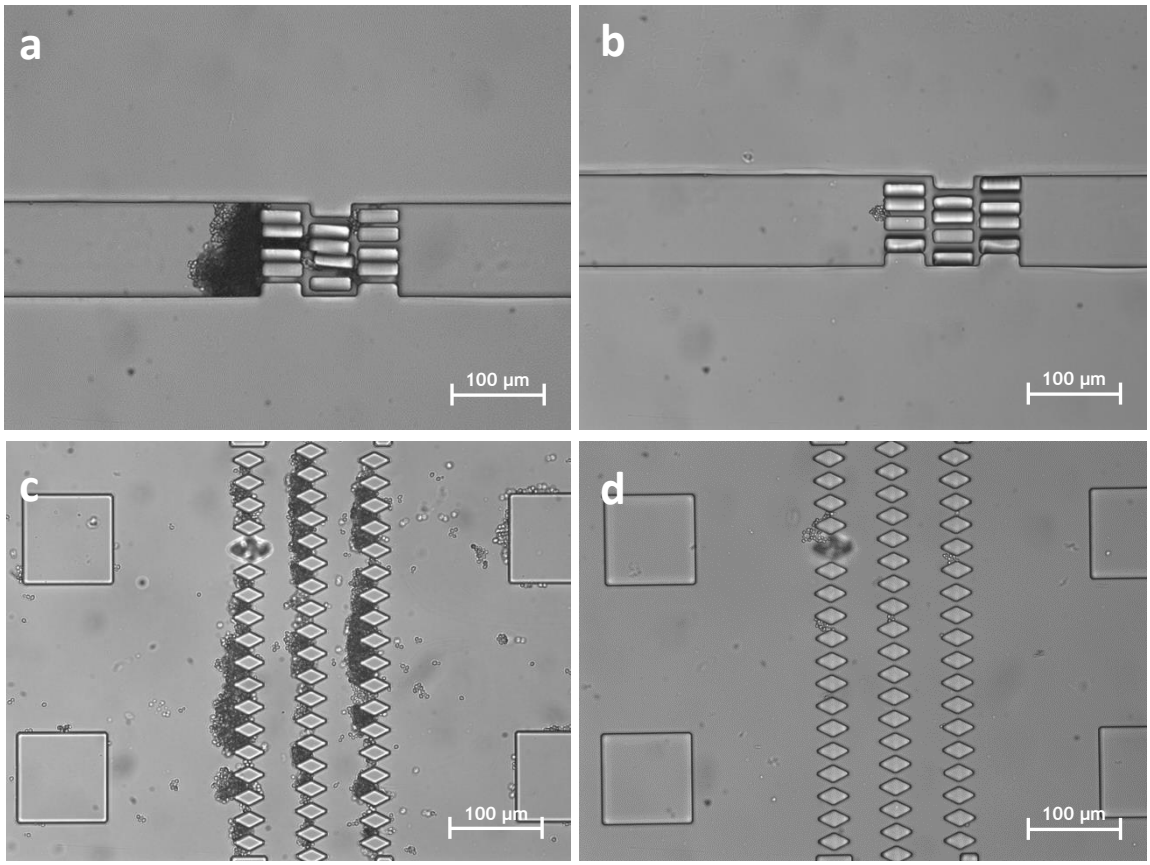

Figure 19 – Cell counting of both retained and non-retained cells in different cell concentrations

For each microchannel 1 µl was introduced at a flow rate of 1µl/minute. In both (a) narrow and (c) widened microchannels, cells were impossible to count when a concentration of 10^4 cells/µl was used; Using a cell concentration of $0.2x10^4$ cells/µl, assessment of total number of cells was possible for (b) narrow and (d) widened microchannels. Original magnification 200x.

While a concentration of approximately 10^4 cells/µl resulted in a significant accumulation of cells in traps (Figure 19 a and c), preventing the counting of cells, the concentration of 10^3 cells/µl led to very few cells, often none, trapped inside the microchannel. Therefore, there was a need to establish an intermediate concentration that allowed a restrict number of cells to pass through the microchannel in a single microliter (as a way to keep the procedure time efficient), being in this way possible to count them and effectively assess the microchannel retention rate. A set of dilutions in ethanol from the 10^4 cells/µl concentration was performed, until a dilution of 5:1 (80% ethanol, 20% initial cell suspension in ethanol, making for a cellular concentration of $0.2x10^4$ cells/µl) allowed to obtain the ideal

results: by introducing a single microliter into the microchannel at 1 µl/minute flow rate, a significant number of cells trapped in the trapping array section were observed while not making their individual counting impossible (Figure 19 b and d).

4.3. Oxygen plasma treatment to the Tygon tube

Considering aforementioned hypothesis that the intended cell concentration was not verified inside the microchannels, the fact that almost no cells were observed stuck in the microchannel before reaching the trapping array section meant that a significant number of cells were possibly being lost in the syringe/tube system. Since polar solvents are used in this procedure (fixed cells are suspended in ethanol), it was proposed that the hydrophobic nature of the Tygon tube could be disrupting the fluid flow and *S. cerevisiae* cells (also of hydrophobic nature due to their high-lipid constituted membrane[156, 157]) were sedimenting inside the tube before reaching the microchannel inlet.

With intention of altering the tube surface to a hydrophilic nature as a way to reduce cell adhesion to the walls, the tube was subjected to plasma treatment with the same protocol applied to the microchannel with PDMS-glass seal. Effectively, by introducing the minimal cell concentration previously set as necessary to assess retention capabilities ($0.2x10^4$ cells/µl), a higher cell number was observed flowing through the microchannel when the tube was submitted to oxygen plasma treatment, although this increase was not as significant as expected.

4.4. Reverse flow system

Even with the newly obtained dilution used in conjunction with oxygen plasma treated Tygon tube, the amount of cells observed reaching the trap sections of the microchannels (less than 100 cells/µl) was still significantly less than the concentration present at the start of the system (nearly 2000 cells/µl). It was then hypothesized that cell agglomerates were still being retained in the tube or in the precision tip used to connect the tube to the microchannel inlet. As such, an alternative system was developed in which the use of the syringe/tube system to introduce the liquids into the microchannel was removed. Instead, the microchannel entry hole was widened in microfabrication, forming a well 2.5 mm wide capable of retaining more than 10 µl of fluid. After the microchannel was submitted to oxygen plasma treatment, an empty syringe/tube apparatus was introduced at the outlet of the microchannel and, when necessary, the flow rate was set to pull 1 µl of fluid per minute. Finally, using a micropipette, the fixed cell suspension was placed into the

inlet well (at least 5 µl to guarantee that at no moment the fluid flow was interrupted, although refilling the well was possible, if necessary). Due to both the hydrophilic treatment and the suction effect provided by the negative flow rate at the outlet of the microchannel, the fluid flowed through the microchannel at the intended flow rate of 1 µl/min. This method for introducing the fluid into the microchannel was named reverse flow system and a schematic comparing it with the regular system is represented in Figure 20.

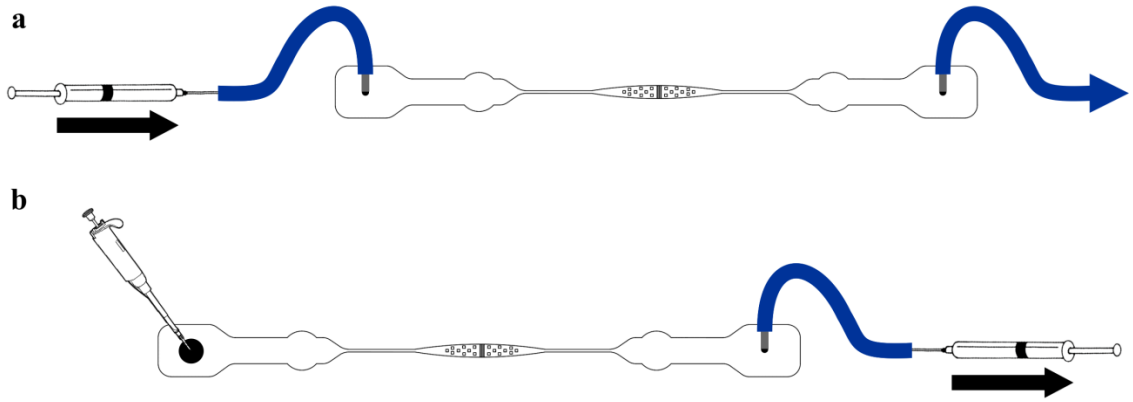

Figure 20 – Schematic of the liquid handling strategies – regular system and reverse flow system

(a) Regular system: the syringe filled with cell suspension is set on a low pressure pump that allows controlling the rate at which the plunger is pushed and, as such, the flow rate inside the microchannel is also controlled. Tygon tubing is used to connect the syringe to the inlet of the microchannel and as an exit to excess fluid at the outlet of the microchannel; (b) Reverse flow system: the inlet hole of the microchannel is widened, being able to hold more than 10 µl of the cell suspension directly introduced with a micropipette. The empty syringe is connected to the outlet of the microchannel with a Tygon tube and then placed on a low pressure pump that controls the rate at which the plunger is pulled, in this way also regulating the flow rate inside the microchannel.

Using the concentration previously set as the minimum necessary to assess retention capabilities ($0.2x10^4$ cells/µl, shown in subchapter IV – 4.2), it was immediately visible that the number of cells reaching the trap section of the microchannels had increased significantly, even with appearance of large agglomerates. Therefore, further dilutions for the minimal cell concentration were possible, decreasing to 10^3 cells/µl (Figure 21).

Besides the advantage of having a lower detection limit, microfluidic experiments using the reverse flow system are significantly easier to perform. As the cell fluid is directly added to the inlet well and the PDMS surface is treated to acquire hydrophilic nature, capillarity effects come into play and the fluid fills the microchannel without need of a pressure driven flow rate. In fact, in this system the syringe pump was only needed to remove the fluid from the microchannel. As such, the syringe pump was used in three instances: to pull the ethanol solution as

hybridization solution was added; to pull the hybridization solution as washing solution entered the microchannel; to remove the washing solution as distilled water was added.

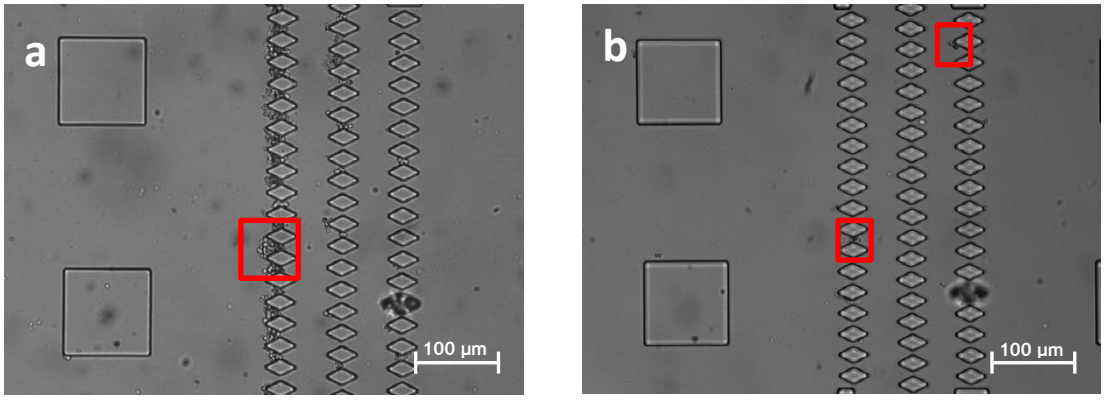

Figure 21 – The reverse flow system effect on the number of cells flowing through the microchannel

(a) Using the reverse flow system to introduce a cell suspension with the previously determined minimal cell concentration, $0.2x10^4$ cells/µl, a significant increase in cell number was observed, as well as agglomerates (marked with the red square) that could otherwise be trapped in the Tygon tube when using the regular system; (b) To allow an effective counting of individual cells (marked with the red squares) when using the reverse flow system, a reduction of concentration to 10^3 cells/µl was applied. Original magnification 200x.

In summary, the reverse flow system with a flow rate of 1 µl/minute and dilution of the cell suspension in ethanol (final concentration of 10^3 cells/µl) was adopted for ensuing experiments, while oxygen plasma tratment of the tubes was no longer necessary and therefore discarded.

5. Influence of focus plane on cell detection

As the following experiments were heavily based on the number and behavior of cells flowing through the microchannel, it was first necessary to assess if all cells were indeed visible at the same focus plane.

By slightly changing the focus plane while maintaining the traps in focus, it was verified that cells in different focus planes are still visible and distinguishable (Figure 22). Since most cells flow near the middle plane of the microchannel where the velocity is higher[158], in microchannels with the preferred depth of 30 µm any focus plane based on the trapping array section allowed to easily identify all cells. For comparison, microchannels with a height of 50 µm presented some problems to individually count cells if they were part of an agglomerate in a different focus plane.

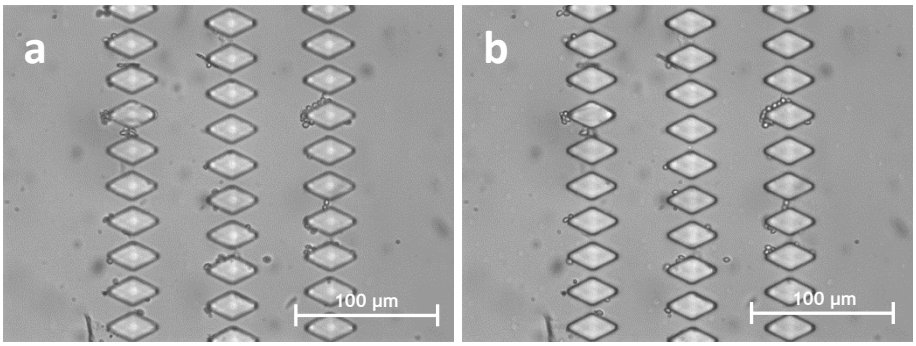

Figure 22 – Effect of focus plane variation in the same microchannel with a depth of 30 µm
Cells are visible and distinguishable in (a) deep or (b) shallow focus planes. Original magnification 400x.

6. Cell retention efficiency

The method used to assess retention capabilities involved filming the trap section of each microchannel (with the 200x magnification for widened microchannels at the trapping array section, 400x for narrow microchannels) at constant flow rate of 1 µl/minute during 1 minute, starting as soon as the solution of 10^3 cells/µl first passed through the trap section. Despite being accessed that microchannels with 30 µm depth were preferable due to presenting fewer microfabrication errors and being easier to observe despite the plain of focus, 30 and 50 µm depths were available for the elongated and pyramid pillar-based microchannels and so retention efficiency was tested on both depths to verify if significant differences in cell retention efficiency were observed. Afterwards, resorting to video software where moving cells were highlighted (Figure 23), the quotient of the total number of cells observed and trapped cells was obtained.

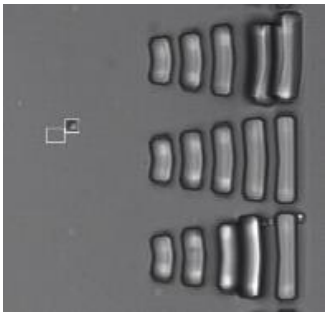

Figure 23 – Detail of video software highlighting a moving cell
Recordings obtained with Leica Application Suite 3.7.0 were used to visually assess retention efficiency of microchannels. VLC media player was used to playback the recording at half speed with motion detection. The white squares added automatically by the VLC detection tool highlight differences between current and previous frames, allowing to easily observe cell movement inside the microchannel. Original magnification 200x.

After at least five repetitions for each microchannel, the resulting mean value represented the retention efficiency of the different designs (Figure 24).

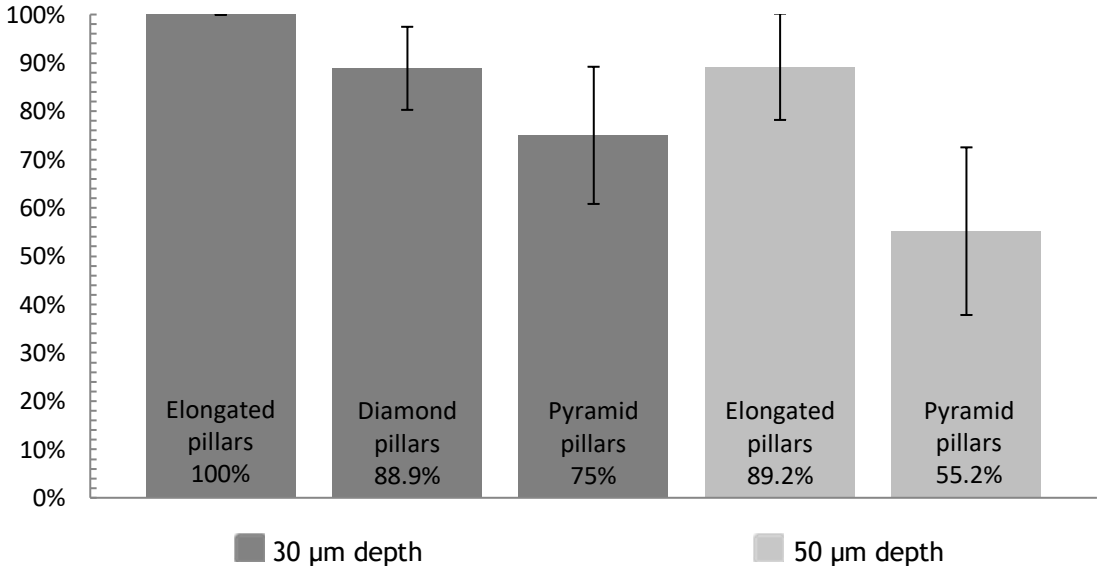

Figure 24 - Cell retention efficiency in the selected trapping array designs

Retention efficiency was assessed by calculating the quotient between the total number of cells observed and cells being trapped in the trapping array section. Microchannels with 30 µm depth presented better results than microchannels with the equivalent trap configuration and 50 µm depth. Overall, the elongated pillar-based design presented higher cell retention efficiency, especially with a depth of 30 µm.

Although all microchannel designs with a 30 µm depth have proven to possess efficiency in cell retention equal or higher than 75%, the elongated pillar-based design should be highlighted due to its perfect retention efficiency. This high efficiency, to a lesser extent also observed in the same design with 50 µm depth, can be credited to the fact that the narrowing sections of these traps (shown in CFD simulations to have a high flow velocity) are 45 µm long and therefore able to gradually reduce the velocity of cells along the trap section. Also, the off-set configuration of the trapping array contributes to this efficiency, as in the chance of a cell being able to flow through the first trap array, it would often encounter a wall from the second trap array and usually stop at that point (where flow velocity is already reduced, as shown in CFD simulations). Alas, it is important to emphasize that these results were obtained with constant fluid flow and although no cells were lost when fluid flow was stopped, this design is highly susceptible to lose cells trapped before the first pillar row due to the fluid reflux that may occur during PNA-FISH incubation steps (with hybridization and washing solutions)[143]. Still, no cells should be able to disengage from the narrowing sections of the trap.

Besides the elongated pillar design, diamond pillar-based design has shown promising results, with a cell retention efficiency of 88.9% with 30 µm depth (the master mold to construct this design with 50 µm depth was not available). As is the case with the elongated pillar-based design, this design has three rows of pillars that have proven to be effective in slowing and the trapping most cells. Because most cells became trapped after the first and second pillar rows, thus being contained between rows, this design is predicted to be efficient in case of fluid reflux.

Finally, pyramid pillar-based microchannels presented the lower retention efficiency of the selected designs, with 75% retention efficiency with 30 µm depth and 55.2% with 50 µm depth. Due to having a single row of pillars 5 µm wide, some cells flowing at higher velocities were not retained. In this case, if fluid flow is stopped or its direction is reversed, the number of cells observed in the trapping array section is severely reduced, as cells can easily detach from a single row trapping section.

7. PNA-FISH in microfluidic environment

7.1. Introduction of PNA-FISH labeled cells in the microchannels and control experiments

Before applying PNA-FISH protocol to cells previously fixed/permeabilized and trapped inside the microchannels, cells were submitted to PNA-FISH protocol in suspension and these fluorescence-labeled cells were introduced into the microchannel. This procedure allowed establishing that visualization of fluorescence-labeled cells located at the trapping array section was possible and, if no fluorescence was observed in subsequent experiments, the problem could only be attributed to the PNA-FISH protocol inside the microchannel. The concentration of 10^4 cells/µl was used as a way to guarantee that cells were present in large number at the trapping array section. As expected, fluorescent signal was observed inside the microchannel and so the subsequent experiments where FISH was applied to cells trapped in the microchannel could be performed.

Also, as it was necessary to introduce hybridization solution, washing solution and distilled water into the microchannel after the cells were retained, an experiment was devised to assess if the traps still allowed a regular fluid flow and if the solution introduced would be in direct contact with all trapped cells. As such, after introducing cell suspension with 10^4 cells/µl, a dye solution (crystal violet) was

introduced alternately with distilled water, being possible to distinguish these fluid phases. Observing the phase between the dye solution and distilled water, no alteration in regular fluid flow was registered, with all cells being effectively stained and not removed from the trapping array section.

Throughout all experiments involving fluorescent signals a G-2A filter (not able to detect the green fluorescent dye attached to the PNA probe employed) was used to confirm that the signal obtained was not due to cell autofluorescence. In all instances, observing cells under the G-2A filter yielded no fluorescence. Still, to prove that the FITC filter sensitive to the fluorophore Alexa Fluor 488 attached to the PNA probe did not detect cell autofluorescence, cells were introduced into microchannels in a high concentration (10^4 cells/µl), thus guaranteeing cell presence in the microchannel. Without applying the PNA-FISH protocol, the microchannels were observed under the FITC filter and no autofluorescence was detected.

Additionally, to demonstrate that the PNA probe did not bind to cell nor microchannel surfaces after the washing step, a scramble probe (with a sequence not specific to *S. cerevisiae*) with the same fluorescent dye (Alexa 488) was used. A high cell concentration (10^4 cells/µl) was introduced into the microchannel and, after hybridization and washing steps, it was observed with the FITC filter. No fluorescence was observed, proving that all non-hybridized probes were removed after the washing step, not adhering to the cell nor PDMS surfaces (Appendix VI – Figure 29).

7.2. PNA-FISH inside microchannels

At this stage of the project, no alterations in regular PNA-FISH in suspension protocol were implemented. Cells introduced into the microchannel were exposed to hybridization and washing solutions at the optimal temperature of the probe used (59 ºC) during the usual time period (1 hour and 30 minutes, respectively). The observed results for each microchannel design are presented in Figure 25.

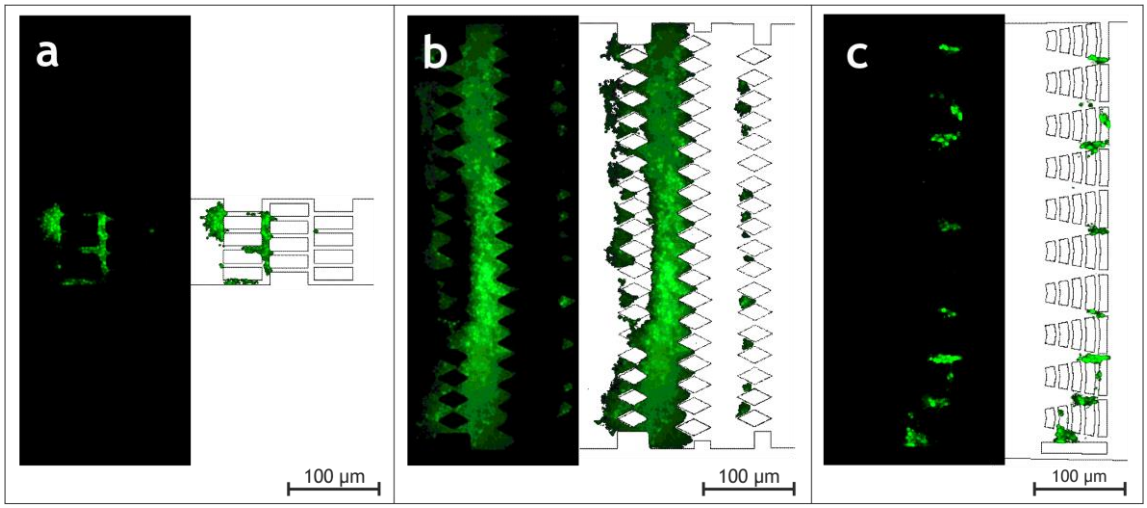

Figure 25 – Signal obtained from executing PNA-FISH protocol to cells trapped in microchannels

The elongated (a), diamond (b) and pyramid (c) pillar-based designs were tested, all with a depth of 30 µm. Images obtained with an inverted epifluorescence microscope are presented, as well as a cutout of the fluorescent cells superimposed on the microchannel designs. Original magnification 200x.

In all three designs, trapped cells presented an effective fluorescent signal. As corroborated by cell retention efficiency tests (subchapter IV - 6), elongated pillar-based design (Figure 25 a) presented an effective retention of cells with fluorescent signal, although not nearly as many cells as the diamond pillar-based design (Figure 25 b). This is due to the fact that most cells are not able to flow through the first row of pillars, therefore accumulating in an area where they are susceptible to become detached when fluid flow is stopped and fluid reflux occurs during the incubation periods of the PNA-FISH protocol (hybridization and washing)[143].

Diamond pillar-based microchannel (Figure 25 b) presents a strong fluorescent signal between the first and second row of trap arrays, corroborating the importance of a sequential barrier design: while the first diamond pillar-based row allows high velocity cells to flow through, cells become trapped in the second pillar row and are unable to flow in the opposite direction during the incubation periods of the FISH protocol.

The problem of cells becoming detached during incubation periods is particularly noticeable in the pyramid pillar-based design (Figure 25 c), since this is the only selected design that presents a single barrier with 5 µm narrow sections to stop the cells while the other two designs have three repeated barriers. Because cell velocity is usually too high for individual cells to be trapped by a single non-elongated trap design and larger cell agglomerates can be removed during incubation periods, only cells trapped between the narrower sections of this design are observed with a fluorescent signal.

Regarding the apparent superior fluorescent signal in the diamond pillar-based design (Figure 25 b), it is important to highlight that, as a way to ensure presence of trapped cells in all designs, the cell suspension used during these experiments presented a concentration of 10^4 cells/µl, which evidently contributed to the success of the only design able to prevent cell loss during incubation periods. While such high cell concentrations are indeed possible in fermentation processes[159], retention efficiency with lower cell concentrations must also be considered, where the diamond pillar-based design is less effective than the elongated pillar-based design (as previously show in cell retention efficiency tests, subchapter IV - 6). Therefore, the fluorescent signal obtained in the elongated pillar-based design (Figure 25 a) should also be considered as a promising result. This design allows an easy identification of the fluorescent signal, as there is a tendency for formation of cell aggregates in a small area of the trapping array region. Also, while in widened microchannels the cells end up widespread across the trapping arrays and thus requiring 200x magnification to observe the entire trapping array section, it is possible to observe the entire trapping array region of a narrow microchannel with the 400x magnification, providing a much more detailed image. Nonetheless, the fact that the elongated pillar-based design lost a high number of cells upon fluid reflux is a clear disadvantage that must be addressed in the forthcoming works, possibly by adding a diamond pillar-based row before the elongated pillars.

V. Conclusions and future work

Conclusions

The PNA-FISH included in microfluidic devices provides several significant improvements over currently existing diagnostic procedures for the food industry, particularly in the quality control area, where rapid and efficient diagnostic procedures are vital[160]. In fact, analysis of the samples retained in a microfluidic device by fluorescence microscopy reduces the amount of support equipment needed, simplifying the procedure and reducing its cost[161]. Also, whereas most diagnostic tools require a pre-enrichment step (as is the case with FISH) and therefore can take a full day to provide results, microfluidic devices work with significantly lower volumes and are able to maintain the diagnostic procedure sensitivity even with no pre-enrichment of the sample, and thus results can be obtained in two to three hours[2, 70].

Unlike other microfluidic devices, this pillar-based system is much less susceptible to clogging[143] and is much simpler to prepare than other systems (e.g. Zhang et al., 2006[162]). Besides the design of these microchannels, the addition of plasma treatment with PDMS-glass seal and development of a new method for introduction of fluids (reverse flow system) greatly contributed to a higher reliability and reduced duration of the microfabrication protocol, reduced probability of air bubble formation and cell adhesion to the PDMS surface, increased number of cells reaching the trapping array region (a relevant aspect of this project since the proposed methodology is intended to work with non-enriched samples) and overall ease of use of the LOCs.

While successful implementation of FISH procedures with animal cells inside microchips has been previously reported by several authors [88, 163-165], the methodology proposed in this masters dissertation poses as an improvement in rapid and easy-to-use diagnostic tools for yeast detection, particularly for use in fermentation-based industries. The presented FISH protocol differs from preceding works as it is able to achieve a significantly higher specificity of detection by using PNA probes[6], being one of the first times that PNA has been applied with considerable success in microchannels using a very simple hydrodynamic method (single straight microchannel with a physical barrier).

Also, although some pillar-based geometries were previously described for use as cell retention methods [166, 167], there are no evidences of geometries similar to the ones described in this work nor do they achieve the retention efficiency observed

with the pillar design of the narrow microchannel with elongated pillars. Strategies for successful retention of yeast cells using U-shape barriers are reported by Li et al. (2004)[168], which constitutes a strategy more difficult to handle since it is highly susceptible to fluid reflux (during hybridization and washing steps required for FISH, fluid flow is stopped and may move in the opposite direction)[143].

The nine microchannel designs provided by Moreira[15] were divided into four categories, depending on the overall microchannel design and disregarding the trapping array section configuration: microchannel 1 is narrow, microchannel 2 is widened and both microchannels 3 and 4 offer different approaches to double inlet designs. From microchannel design 1 (narrow) only the trap configuration in 1b (elongated pillar-based) presented reliable structures upon microfabrication, with design 2a being discarded. Microchannel design 2 (narrow) presented frequent microfabrication errors with trapping array configuration 2a, therefore only 2b (diamond pillar-based) and 2c (pyramid pillar-based) were used. Finally, considering the aim to create an easily reproducible method, both double inlet microchannel designs were discarded for their innate higher handling complexity, which would increase the amount of variables to examine at this early stage of the project. Still, it was possible to observe that the double inlet design 3 allows to effectively limit fluid flow to a single side of the microchannel, while the double inlet design 4 can restrict the fluid flow along the middle plane of the microchannel (crucial for the success of a single horse-shoe trap design).

Throughout the experiments presented in this dissertation, design 1b (elongated pillar-based) with 30 µm depth demonstrated the most promising results: microfabrication errors were rarely observed, cell retention efficiency was very high and the fluorescent signal when combined with PNA-FISH was easy to observe in detail. Still, there is room for improvement, especially regarding to the susceptibility of this design to fluid reflux.

Overall, the PNA-FISH procedure adapted to the microfluidic system proved to be successful, marking *S. cerevisiae* cells previously retained in a microchannel with the intended fluorescent signal, while still presenting development potential.

Future work

Based on the learnings provided by this dissertation, future work may primarily rely on the development of an improved microchannel design combining advantageous characteristics identified in several microchannels: narrow as to facilitate detection of signal during microscopic visualization, maximum height of 30 µm to avoid microfabrication errors, three or more rows of pillars in off-set disposition and pillars at least 15 µm wide (also to reduce occurrence of microfabrication errors) and close to 45 µm long to gradually reduce cells velocity until they become retained. In a new microchannel design, the first row of pillars should allow passage of cells but block them from being dragged backwards when fluid flow is stopped and reflux occurs, which could be achieved with a pillar row with a design similar to the diamond-shaped pillar. Since in single inlet/outlet designs it is difficult to verify the microchannel orientation without a microscope, the same pillar row should be placed at the end of the trap array, making the design symmetric and thus usable when the fluid is introduced from either side. Still, fluid reflux may be prevented in the currently available designs by placing the microchip on a heating plate, surpassing the need to stop the fluid flow when moving the microchip to an incubator, ultimately allowing to achieve the intended incubation temperatures while maintaining a constant fluid flow.

Further investigation on double inlet microchannel configuration is also necessary[169], accessing if their overall process efficacy is superior to that of single inlet designs, to a point that the added complexity of handling a double inlet design might become acceptable.

While the proposed method is already effective in detection of the targeted yeast, an additional reliability should allow quantification of yeasts in the sample, which is particularly useful for fermentation industries to allow differentiation between fermenting and spoilage yeasts[170]. As such, further optimization of the PNA-FISH protocol adapted for microfluidic environment is recommended[70, 171, 172], aiming to balance the ease-of-use with an optimal signal-to-noise ratio. The procedure where the microchip is incubated during hybridization and washing steps must be explored as to increase its reliability, assuring that no air bubbles are formed inside the microchannel. Additional experiments should also entail the execution of fixation/permeabilization step to cells trapped in the microchannels. In this case, since it was already verified that non-fixed cells allow a lower cell

concentration limit necessary for efficient detection, minimal cell concentration tests must be repeated.

In a later stage of the project, use of different nucleic acid mimic probes should also be considered, allowing the microfluidic device to be tested with other microorganisms similar in size to that of *S. cerevisiae*, eventually making the proposed microchannel designs valid for additional applications[173, 174].

Ultimately, the resulting microchip must aim to be viable for use outside of a laboratory environment, allowing in-site testing without necessarily requiring handling by experts in detection methods. With this in mind, an alternative method for fluid handling not requiring a syringe pump should be devised. Additionally, a reliable packaging method must be developed, including the microchip and FISH solutions, and offering clear and easy to follow instructions. The microchip package should also require a vacuum seal, low temperatures and/or liquid environment, as to maintain the hydrophilic capabilities added during microfabrication by oxygen plasma treatment[127].

References

1. Giraffa, G. and D. Carminati, "Molecular techniques in food fermentation: principles and applications", in *Molecular techniques in the microbial ecology of fermented foods*. 2008, Springer. p. 1-30.

2. Rohde, A., *et al.*, "FISHing for bacteria in food–A promising tool for the reliable detection of pathogenic bacteria?" Food microbiol., 2015. **46**: p. 395-407.

3. Xufre, A., *et al.*, "Application of fluorescence in situ hybridisation (FISH) to the analysis of yeast population dynamics in winery and laboratory grape must fermentations." International journal of food microbiology, 2006. **108**(3): p. 376-384.

4. Nielsen, P.E., *et al.*, "Sequence-selective recognition of DNA by strand displacement with a thymine-substituted polyamide." Science, 1991. **254**(5037): p. 1497-1500.

5. Nielsen, P.E., "Peptide nucleic acid: a versatile tool in genetic diagnostics and molecular biology." Current Opinion in Biotechnology, 2001. **12**(1): p. 16-20.

6. Cerqueira, L., *et al.*, "DNA mimics for the rapid identification of microorganisms by fluorescence in situ hybridization (FISH)." Int. J. Mol. Sci., 2008. **9**(10): p. 1944-1960.

7. Morgan, H., D. Holmes, and N.G. Green, "3D focusing of nanoparticles in microfluidic channels." IEE Proceedings-Nanobiotechnology, 2003. **150**(2): p. 76-81.

8. Young, E.W. and D.J. Beebe, "Fundamentals of microfluidic cell culture in controlled microenvironments." Chemical Society Reviews, 2010. **39**(3): p. 1036-1048.

9. Heo, J. and S.Z. Hua, "An overview of recent strategies in pathogen sensing." Sensors, 2009. **9**(6): p. 4483-4502.

10. Yeo, S.F. and B. Wong, "Current status of nonculture methods for diagnosis of invasive fungal infections." Clinical microbiology reviews, 2002. **15**(3): p. 465-484.

11. Xi, C., S.A. Boppart, and L. Raskin, "Use of molecular beacons for the detection of bacteria in microfluidic devices." Microfluidics, BioMEMS, and Medical Microsystems, 2003. **4982**: p. 170-177.

12. Devadhasan, J.P., S. Kim, and J. An, "Fish-on-a-chip: a sensitive detection microfluidic system for alzheimer's disease." Journal of biomedical science, 2011. **18**(1): p. 33.

13. Feldmann, H., "Yeast: molecular and cell biology." 2011: John Wiley & Sons.

14. Perry-O'Keefe, H., *et al.*, "Identification of indicator microorganisms using a standardized PNA FISH method." Journal of microbiological methods, 2001. **47**(3): p. 281-292.

15. Moreira, D., "Integration of Microfluidics and Fluorescence *In Situ* Hybridization (FISH) for the Rapid Identification of Microorganisms." Dissertation for Masters Degree in Bioengineering, 2014. Faculty of Engineering of University of Porto.

16. Choi, M.J., *et al.*, "Micropattern array with gradient size (μPAGS) plastic surfaces fabricated by PDMS (polydimethylsiloxane) mold-based hot embossing technique for investigation of cell–surface interaction." Biofabrication, 2012. **4**(4): p. 045006.

17. Bodas, D. and C. Khan-Malek, "Formation of more stable hydrophilic surfaces of PDMS by plasma and chemical treatments." Microelectronic engineering, 2006. **83**(4-9): p. 1277-1279.

18. Robinson, R.K. and C.A. Batt, "Encyclopedia of food microbiology." 1999: Academic press.

19. Lavoisier, A.L., "Opuscules physiques et chimiques." 1801: Deterville.

20. Brock, T.D., "Milestones in Microbiology." Academic Medicine, 1961. **36**(7): p. 847.

21. Alba-Lois, L. and C. Segal-Kischinevzky, "Yeast fermentation and the making of beer and wine." Nature Education, 2010. **3**(9): p. 17.

22. Schmidt, F., "Optimization and scale up of industrial fermentation processes." Applied microbiology and biotechnology, 2005. **68**(4): p. 425-435.

23. Legras, J.L., *et al.*, "Bread, beer and wine: Saccharomyces cerevisiae diversity reflects human history." Molecular ecology, 2007. **16**(10): p. 2091-2102.

24. Ostergaard, S., L. Olsson, and J. Nielsen, "Metabolic engineering of Saccharomyces cerevisiae." Microbiology and Molecular Biology Reviews, 2000. **64**(1): p. 34-50.

25. Fugelsang, K.C. and C.G. Edwards, "Wine microbiology: practical applications and procedures." 2006: Springer Science & Business Media.

26. Birch, A.N., *et al.*, "Influence of commercial baker's yeasts on bread aroma profiles." Food Research International, 2013. **52**(1): p. 160-166.

27. Loureiro, V.l., "Spoilage yeasts in foods and beverages: characterisation and ecology for improved diagnosis and control." Food Research International, 2000. **33**(3): p. 247-256.

28. Loureiro, V. and M. Malfeito-Ferreira, "Spoilage yeasts in the wine industry." International journal of food microbiology, 2003. **86**(1): p. 23-50.

29. Loureiro, V. and A. Querol, "The prevalence and control of spoilage yeasts in foods and beverages." Trends in Food Science & Technology, 1999. **10**(11): p. 356-365.

30. Camarasa, C., *et al.*, "Phenotypic landscape of Saccharomyces cerevisiae during wine fermentation: evidence for origin-dependent metabolic traits." PloS one, 2011. **6**(9): p. e25147.

31. Su, Y., *et al.*, "Phenotypic and genomic differences among S. cerevisiae strains in nitrogen requirements during wine fermentations." Food Microbiology, 2021. **96**: p. 103685.

32. Hay, R.J. and R.M. Jones, "New molecular tools in the diagnosis of superficial fungal infections." Clinics in dermatology, 2010. **28**(2): p. 190-196.

33. Adeyemo, S. and A. Onilude, "Molecular identification of Lactobacillus plantarum isolated from fermenting cereals." International Journal of Biotechnology and Molecular Biology Research, 2014. **5**(6): p. 59-67.

34. Bagheripoor-Fallah, N., *et al.*, "Comparison of molecular techniques with other methods for identification and enumeration of probiotics in fermented milk products." Critical reviews in food science and nutrition, 2015. **55**(3): p. 396-413.

35. Gracias, K.S. and J.L. McKillip, "A review of conventional detection and enumeration methods for pathogenic bacteria in food." Canadian journal of microbiology, 2004. **50**(11): p. 883-890.

36. Kurtzman, C.P., *et al.*, "Methods for isolation, phenotypic characterization and maintenance of yeasts." The yeasts, a taxonomic study, 5th edn. Elsevier, Amsterdam, 2011: p. 87-110.

37. Hierro, N., *et al.*, "New PCR-based methods for yeast identification." Journal of applied microbiology, 2004. **97**(4): p. 792-801.

38. Sabate, J., *et al.*, "Isolation and identification of yeasts associated with vineyard and winery by RFLP analysis of ribosomal genes and mitochondrial DNA." Microbiological research, 2002. **157**(4): p. 267-274.

39. Quesada, M. and J. Cenis, "Use of random amplified polymorphic DNA (RAPD-PCR) in the characterization of wine yeasts." American Journal of Enology and Viticulture, 1995. **46**(2): p. 204-208.

40. Schochetman, G., C.-Y. Ou, and W.K. Jones, "Polymerase chain reaction." The Journal of infectious diseases, 1988: p. 1154-1157.

41. Marklein, G., *et al.*, "Matrix-assisted laser desorption ionization-time of flight mass spectrometry for fast and reliable identification of clinical yeast isolates." Journal of clinical microbiology, 2009. **47**(9): p. 2912-2917.

42. Amann, R. and B.M. Fuchs, "Single-cell identification in microbial communities by improved fluorescence in situ hybridization techniques." Nature Rev. Microbiol., 2008. **6**(5): p. 339-348.

43. Amann, R. and W. Ludwig, "Ribosomal RNA-targeted nucleic acid probes for studies in microbial ecology." FEMS Microbiology Reviews, 2000. **24**(5): p. 555-565.

44. Stender, H., *et al.*, "Identification of Dekkera bruxellensis (Brettanomyces) from wine by fluorescence in situ hybridization using peptide nucleic acid probes." Applied and environmental microbiology, 2001. **67**(2): p. 938-941.

45. Moter, A. and U.B. Göbel, "Fluorescence in situ hybridization (FISH) for direct visualization of microorganisms." Journal of microbiological methods, 2000. **41**(2): p. 85-112.

46. Rocha, R., C. Almeida, and N.F. Azevedo, "Influence of the fixation/permeabilization step on peptide nucleic acid fluorescence in situ hybridization (PNA-FISH) for the detection of bacteria." PloS one, 2018. **13**(5): p. e0196522.

47. Wagner, M., M. Horn, and H. Daims, "Fluorescence in situ hybridisation for the identification and characterisation of prokaryotes." Current opinion in microbiology, 2003. **6**(3): p. 302-309.

48. Spector, D.L. and R.D. Goldman, "Basic methods in microscopy: protocols and concepts from cells: a laboratory manual." 2006: Cold Spring Harbor Laboratory Press New York.

49. Javois, L.C., "Immunocytochemical methods and protocols." Vol. **115**. 1999: Springer.

50. McLEAN, I.W. and P.K. NAKANE, "Periodate-lysine-paraformaldehyde fixative a new fixative for immunoelectron microscopy." Journal of Histochemistry & Cytochemistry, 1974. **22**(12): p. 1077-1083.

51. Bancroft, J.D. and M. Gamble, "Theory and practice of histological techniques." 2008: Elsevier Health Sciences.

52. Jamur, M.C. and C. Oliver, "Permeabilization of cell membranes", in *Immunocytochemical methods and protocols*. 2010, Springer. p. 63-66.

53. Warner, J.R., "The economics of ribosome biosynthesis in yeast." Trends in biochemical sciences, 1999. **24**(11): p. 437-440.

54. Eckenrode, V.K., J. Arnold, and R.B. Meagher, "Comparison of the nucleotide sequence of soybean 18S rRNA with the sequences of other small-subunit rRNAs." Journal of Molecular Evolution, 1985. **21**(3): p. 259-269.

55. Veldman, G.M., *et al.*, "The primary and secondary structure of yeast 26S rRNA." Nucleic Acids Research, 1981. **9**(24): p. 6935-6952.

56. Guimaraes, N., *et al.*, "Development and application of a novel peptide nucleic acid probe for the specific detection of Helicobacter pylori in gastric biopsy specimens." Journal of clinical microbiology, 2007. **45**(9): p. 3089-3094.

57. Bayani, J. and J.A. Squire, "Application and interpretation of FISH in biomarker studies." Cancer letters, 2007. **249**(1): p. 97-109.

58. Rogers, S.W., T.B. Moorman, and S.K. Ong, "Fluorescent in situ hybridization and micro-autoradiography applied to ecophysiology in soil." Soil Science Society of America Journal, 2007. **71**(2): p. 620-631.

59. Miyauchi, R., *et al.*, "Diversity of nitrite reductase genes in "Candidatus Accumulibacter phosphatis"-dominated cultures enriched by flow-cytometric sorting." Applied and environmental microbiology, 2007. **73**(16): p. 5331-5337.

60. Catalina, P., *et al.*, "Conventional and molecular cytogenetic diagnostic methods in stem cell research: a concise review." Cell biology international, 2007. **31**(9): p. 861-869.

61. DeLong, E.F., G.S. Wickham, and N.R. Pace, "Phylogenetic stains: ribosomal RNA-based probes for the identification of single cells." Science, 1989. **243**(4896): p. 1360-1363.

62. Forrest, G., *et al.*, "Peptide nucleic acid fluorescence in situ hybridization-based identification of Candida albicans and its impact on mortality and antifungal therapy costs." Journal of clinical microbiology, 2006. **44**(9): p. 3381-3383.

63. Wahlestedt, C., *et al.*, "Potent and nontoxic antisense oligonucleotides containing locked nucleic acids." Proceedings of the National Academy of Sciences, 2000. **97**(10): p. 5633-5638.

64. Lomakin, A. and M.D. Frank-Kamenetskii, "A theoretical analysis of specificity of nucleic acid interactions with oligonucleotides and peptide nucleic acids (PNAs)." Journal of molecular biology, 1998. **276**(1): p. 57-70.

65. Shakeel, S., S. Karim, and A. Ali, "Peptide nucleic acid (PNA)—a review." Journal of Chemical Technology and Biotechnology, 2006. **81**(6): p. 892-899.

66. Orum, H., *et al.*, "Sequence-specific purification of nucleic acids by PNA-controlled hybrid selection." BioTechniques, 1995. **19**(3): p. 472-480.

67. Drobniewski, F., P. More, and G. Harris, "Differentiation of Mycobacterium tuberculosis complex and nontuberculous mycobacterial liquid cultures by using peptide nucleic acid-fluorescence in situ hybridization probes." Journal of clinical microbiology, 2000. **38**(1): p. 444-447.

68. Gildea, B.D., *et al.*, "PNA solubility enhancers." Tetrahedron Letters, 1998. **39**(40): p. 7255-7258.

69. Stager, C.E. and J. Davis, "Automated systems for identification of microorganisms." Clinical microbiology reviews, 1992. **5**(3): p. 302-327.

70. Huber, D., L.V. von Voithenberg, and G. Kaigala, "Fluorescence in situ hybridization (FISH): history, limitations and what to expect from micro-scale FISH?" Micro and Nano Engineering, 2018. **1**: p. 15-24.

71. Hultén, M.A., S. Dhanjal, and B. Pertl, "Rapid and simple prenatal diagnosis of common chromosome disorders: advantages and disadvantages of the molecular methods FISH and QF-PCR." Reproduction, 2003. **126**(3): p. 279-297.

72. Stone, H.A., A.D. Stroock, and A. Ajdari, "Engineering flows in small devices: microfluidics toward a lab-on-a-chip." Annu. Rev. Fluid Mech., 2004. **36**: p. 381-411.

73. Kleinstreuer, C., "Microfluidics and nanofluidics: theory and selected applications." 2013: John Wiley & Sons.

74. Sia, S.K. and G.M. Whitesides, "Microfluidic devices fabricated in poly (dimethylsiloxane) for biological studies." Electrophoresis, 2003. **24**(21): p. 3563-3576.

75. Damean, N., P.P. Regtien, and M. Elwenspoek, "Heat transfer in a MEMS for microfluidics." Sensors and Actuators A: Physical, 2003. **105**(2): p. 137-149.

76. Rott, N., "Note on the history of the Reynolds number." Annual review of fluid mechanics, 1990. **22**(1): p. 1-12.

77. Karimi, A., S. Yazdi, and A. Ardekani, "Hydrodynamic mechanisms of cell and particle trapping in microfluidics." Biomicrofluidics, 2013. **7**(2): p. 021501.

78. Munson, B.R., *et al.*, "Fluid mechanics." 2013: Wiley Singapore.

79. Wang, Q., D. Yuan, and W. Li, "Analysis of hydrodynamic mechanism on particles focusing in micro-channel flows." Micromachines, 2017. **8**(7): p. 197.

80. Stone, H.A. and S. Kim, "Microfluidics: basic issues, applications, and challenges." AIChE Journal, 2001. **47**(6): p. 1250-1254.

81. Mitchell, P., "Microfluidics-downsizing large-scale biology." Nature biotechnology, 2001. **19**(8): p. 717-721.

82. Squires, T.M. and S.R. Quake, "Microfluidics: Fluid physics at the nanoliter scale." Reviews of modern physics, 2005. **77**(3): p. 977.

83. Aniskin, V.M., K.V. Adamenko, and A.A. Maslov, "Internal pressure measurements in microchannels of different shapes." 2011.

84. Einstein, A., "Investigations on the Theory of the Brownian Movement." 1956: Courier Corporation.

85. Kholodenko, A.L. and J.F. Douglas, "Generalized Stokes-Einstein equation for spherical particle suspensions." Physical Review E, 1995. **51**(2): p. 1081.

86. Beebe, D.J., G.A. Mensing, and G.M. Walker, "Physics and applications of microfluidics in biology." Annual review of biomedical engineering, 2002. **4**(1): p. 261-286.

87. Thorsen, T., S.J. Maerkl, and S.R. Quake, "Microfluidic large-scale integration." Science, 2002. **298**(5593): p. 580-584.

88. Sieben, V., *et al.*, "FISH and chips: Chromosomal analysis on microfluidic platforms." IET Nanobiotechnol., 2007. **1**(3): p. 27-35.

89. Nguyen, H.-T., *et al.*, "Low-cost, accessible fabrication methods for microfluidics research in low-resource settings." Micromachines, 2018. **9**(9): p. 461.

90. Erickson, D., "Towards numerical prototyping of labs-on-chip: modeling for integrated microfluidic devices." Microfluidics and Nanofluidics, 2005. **1**(4): p. 301-318.

91. Chung, T., "Computational fluid dynamics." 2010: Cambridge university press.

92. Andersson, B., *et al.*, "Computational fluid dynamics for engineers." 2011: Cambridge University Press.

93. Versteeg, H.K. and W. Malalasekera, "An introduction to computational fluid dynamics: the finite volume method." 2007: Pearson Education.

94. Nilsson, J., *et al.*, "Review of cell and particle trapping in microfluidic systems." Analytica chimica acta, 2009. **649**(2): p. 141-157.

95. Moorthy, J. and D.J. Beebe, "In situ fabricated porous filters for microsystems." Lab on a Chip, 2003. **3**(2): p. 62-66.

96. Karwa, M., D. Hahn, and S. Mitra, "A sol–gel immobilization of nano and micron size sorbents in poly (dimethylsiloxane)(PDMS) microchannels for microscale solid phase extraction (SPE)." Analytica chimica acta, 2005. **546**(1): p. 22-29.

97. Laun, P., *et al.*, "Aged mother cells of Saccharomyces cerevisiae show markers of oxidative stress and apoptosis." Molecular microbiology, 2001. **39**(5): p. 1166-1173.

98. Di Carlo, D., N. Aghdam, and L.P. Lee, "Single-cell enzyme concentrations, kinetics, and inhibition analysis using high-density hydrodynamic cell isolation arrays." Analytical chemistry, 2006. **78**(14): p. 4925-4930.

99. Narayanamurthy, V., *et al.*, "Microfluidic hydrodynamic trapping for single cell analysis: mechanisms, methods and applications." Analytical Methods, 2017. **9**(25): p. 3751-3772.

100. Andersson, H., *et al.*, "Micromachined flow-through filter-chamber for chemical reactions on beads." Sensors and Actuators B: Chemical, 2000. **67**(1): p. 203-208.

101. Madou, M.J., "Fundamentals of microfabrication: the science of miniaturization." 2018: CRC press.

102. Whitesides, G.M., "The origins and the future of microfluidics." Nature, 2006. **442**(7101): p. 368-373.

103. Xia, Y., *et al.*, "Replica molding using polymeric materials: A practical step toward nanomanufacturing." Advanced Materials, 1997. **9**(2): p. 147-149.

104. Weibel, D.B., W.R. DiLuzio, and G.M. Whitesides, "Microfabrication meets microbiology." Nature Reviews Microbiology, 2007. **5**(3): p. 209-218.

105. McDonald, J.C. and G.M. Whitesides, "Poly (dimethylsiloxane) as a material for fabricating microfluidic devices." Accounts of chemical research, 2002. **35**(7): p. 491-499.

106. Xia, Y., *et al.*, "Non-photolithographic methods for fabrication of elastomeric stamps for use in microcontact printing." Langmuir, 1996. **12**(16): p. 4033-4038.

107. Anderson, J.R., *et al.*, "Fabrication of topologically complex three-dimensional microfluidic systems in PDMS by rapid prototyping." Analytical chemistry, 2000. **72**(14): p. 3158-3164.

108. Hansen, A.S., N. Hao, and E.K. O'shea, "High-throughput microfluidics to control and measure signaling dynamics in single yeast cells." Nature protocols, 2015. **10**(8): p. 1181-1197.

109. Haverkorn von Rijsewijk H.C., L.P.E.J., and Thomas G.E., "Cast molding on the micrometer scale." Philips Tech. Rev., 1982. **40**: p. 287-297.

110. Xia, Y. and G.M. Whitesides, "Soft lithography." Annu. Rev. Mater. Sci., 1998. **28**(1): p. 153-184.

111. Kuncova-Kallio, J. and P.J. Kallio, "PDMS and its suitability for analytical microfluidic devices." 2006 International Conference of the IEEE Engineering in Medicine and Biology Society, 2006: p. 2486-2489.

112. Becker, H. and L.E. Locascio, "Polymer microfluidic devices." Talanta, 2002. **56**(2): p. 267-287.

113. Bowen, J., D. Cheneler, and A. Robinson, "Direct e-beam lithography of PDMS." Microelectronic Engineering, 2012. **97**: p. 34-37.

114. Mata, A., A.J. Fleischman, and S. Roy, "Characterization of polydimethylsiloxane (PDMS) properties for biomedical micro/nanosystems." Biomedical microdevices, 2005. **7**(4): p. 281-293.

115. Toepke, M.W. and D.J. Beebe, "PDMS absorption of small molecules and consequences in microfluidic applications." Lab Chip, 2006. **6**(12): p. 1484-1486.

116. Gonsalves, K.E., "Inorganic polymers." Advanced Materials, 1993. **5**(1): p. 63-63.

117. Bhagat, A.A.S., P. Jothimuthu, and I. Papautsky, "Photodefinable polydimethylsiloxane (PDMS) for rapid lab-on-a-chip prototyping." Lab on a Chip, 2007. **7**(9): p. 1192-1197.

118. Makamba, H., *et al.*, "Surface modification of poly (dimethylsiloxane) microchannels." Electrophoresis, 2003. **24**(21): p. 3607-3619.

119. Efimenko, K., W.E. Wallace, and J. Genzer, "Surface modification of Sylgard-184 poly (dimethyl siloxane) networks by ultraviolet and ultraviolet/ozone treatment." Journal of colloid and interface science, 2002. **254**(2): p. 306-315.

120. Hillborg, H. and U. Gedde, "Hydrophobicity recovery of polydimethylsiloxane after exposure to corona discharges." Polymer, 1998. **39**(10): p. 1991-1998.

121. Tóth, A., *et al.*, "Oxidative damage and recovery of silicone rubber surfaces. I. X-ray photoelectron spectroscopic study." Journal of applied polymer science, 1994. **52**(9): p. 1293-1307.

122. Kakuta, M., F.G. Bessoth, and A. Manz, "Microfabricated devices for fluid mixing and their application for chemical synthesis." The Chemical Record, 2001. **1**(5): p. 395-405.

123. Wu, D., J. Qin, and B. Lin, "Self-assembled epoxy-modified polymer coating on a poly (dimethylsiloxane) microchip for EOF inhibition and biopolymers separation." Lab on a Chip, 2007. **7**(11): p. 1490-1496.

124. Hillborg, H., *et al.*, "Crosslinked polydimethylsiloxane exposed to oxygen plasma studied by neutron reflectometry and other surface specific techniques." Polymer, 2000. **41**(18): p. 6851-6863.

125. Hong, S.M., *et al.*, "Hydrophilic surface modification of PDMS using atmospheric RF plasma." Journal of physics: conference series, 2006. **34**(1): p. 656.

126. Ruben, B., *et al.*, "Oxygen plasma treatments of polydimethylsiloxane surfaces: effect of the atomic oxygen on capillary flow in the microchannels." Micro & Nano Letters, 2017. **12**(10): p. 754-757.

127. Tan, S.H., *et al.*, "Oxygen plasma treatment for reducing hydrophobicity of a sealed polydimethylsiloxane microchannel." Biomicrofluidics, 2010. **4**(3): p. 032204.

128. Eddington, D.T., J.P. Puccinelli, and D.J. Beebe, "Thermal aging and reduced hydrophobic recovery of polydimethylsiloxane." Sensors and Actuators B: Chemical, 2006. **114**(1): p. 170-172.

129. Kim, J., *et al.*, "The mechanisms of hydrophobic recovery of polydimethylsiloxane elastomers exposed to partial electrical discharges." Journal of colloid and interface science, 2001. **244**(1): p. 200-207.

130. Chen, I.-J. and E. Lindner, "The stability of radio-frequency plasma-treated polydimethylsiloxane surfaces." Langmuir, 2007. **23**(6): p. 3118-3122.

131. Hashimoto, M., *et al.*, "Formation of Bubbles and Droplets in Parallel, Coupled Flow-Focusing Geometries." Small, 2008. **4**(10): p. 1795-1805.

132. Morra, M., *et al.*, "On the aging of oxygen plasma-treated polydimethylsiloxane surfaces." Journal of Colloid and Interface Science, 1990. **137**(1): p. 11-24.

133. Bodas, D. and C. Khan-Malek, "Hydrophilization and hydrophobic recovery of PDMS by oxygen plasma and chemical treatment—An SEM investigation." Sensors and Actuators B: Chemical, 2007. **123**(1): p. 368-373.

134. Bhattacharya, S., *et al.*, "Studies on surface wettability of poly (dimethyl) siloxane (PDMS) and glass under oxygen-plasma treatment and correlation with bond strength." Microelectromechanical Systems, Journal of, 2005. **14**(3): p. 590-597.

135. Oláh, A. and G.J. Vancso, "Characterization of adhesion at solid surfaces: Development of an adhesion-testing device." European polymer journal, 2005. **41**(12): p. 2803-2823.

136. Ibáñez-Ibáñez, P.F., *et al.*, "Contact line relaxation of sessile drops on PDMS surfaces: A methodological perspective." Journal of Colloid and Interface Science, 2021. **589**: p. 166-172.

137. Law, K.-Y., "Definitions for hydrophilicity, hydrophobicity, and superhydrophobicity: getting the basics right". 2014, ACS Publications. p. 686-688.

138. Mark, D., *et al.*, "Microfluidic lab-on-a-chip platforms: requirements, characteristics and applications." Chemical Society Reviews, 2010. **39**(3): p. 1153-1182.

139. Vowell, S., "Microfluidics Effects of Surface Tension." Physics, 2009. **486**.

140. Larsson, C., *et al.*, "Growth and metabolism of Saccharomyces cerevisiae in chemostat cultures under carbon-, nitrogen-, or carbon-and nitrogen-limiting conditions." Journal of bacteriology, 1993. **175**(15): p. 4809-4816.

141. Andorra, I., *et al.*, "Analysis and direct quantification of *Saccharomyces cerevisiae* and *Hanseniaspora guilliermondii* populations during alcoholic fermentation by fluorescence in situ hybridization, flow cytometry and quantitative PCR." Food microbiol., 2011. **28**(8): p. 1483-1491.

142. Lima, C., "Application of response surface methodology (RSM) to optimize the hybridization efficiency of a PNA probe targeting *Saccharomyces cerevisiae*." Dissertation for Masters Degree in Bioengineering, 2013. Faculty of Engineering of University of Porto.

143. Meireles, F., "PNA-FISH with microfluidics." Dissertation for Masters Degree in Bioengineering, 2012. Faculty of Engineering of University of Porto.

144. Ashelford, K.E., A.J. Weightman, and J.C. Fry, "PRIMROSE: a computer program for generating and estimating the phylogenetic range of 16S rRNA oligonucleotide probes and primers in conjunction with the RDP-II database." Nucleic acids research, 2002. **30**(15): p. 3481-3489.

145. Yilmaz, L.S. and D.R. Noguera, "Mechanistic approach to the problem of hybridization efficiency in fluorescent in situ hybridization." Applied and environmental microbiology, 2004. **70**(12): p. 7126-7139.

146. Fallahi, H., *et al.*, "Flexible microfluidics: Fundamentals, recent developments, and applications." Micromachines, 2019. **10**(12): p. 830.

147. Jung, G.-Y., *et al.*, "Vapor-phase self-assembled monolayer for improved mold release in nanoimprint lithography." Langmuir, 2005. **21**(4): p. 1158-1161.

148. Freire, M.G., *et al.*, "Surface tensions of imidazolium based ionic liquids: anion, cation, temperature and water effect." Journal of colloid and interface science, 2007. **314**(2): p. 621-630.

149. Olanrewaju, A., *et al.*, "Capillary microfluidics in microchannels: from microfluidic networks to capillaric circuits." Lab on a Chip, 2018. **18**(16): p. 2323-2347.

150. Stender, H., "PNA FISH: an intelligent stain for rapid diagnosis of infectious diseases." Expert review of molecular diagnostics, 2003. **3**(5): p. 649-655.

151. National Center for Biotechnology Information (2021). "PubChem Compound Summary for CID 702, Ethanol." Retrieved October 22, 2021, from: https://pubchem.ncbi.nlm.nih.gov/compound/Ethanol.

152. Thomas Scientific. (2021). "Phosphate Buffer Solution." Retrieved October 22, 2021, from: https://thomassci.com/scientific-supplies/Phosphate-Buffer-Solution.

153. Yilmaz, L.Ş., H.E. Ökten, and D.R. Noguera, "Making all parts of the 16S rRNA of Escherichia coli accessible in situ to single DNA oligonucleotides." Applied and environmental microbiology, 2006. **72**(1): p. 733-744.

154. Fontenete, S., *et al.*, "Prediction of melting temperatures in fluorescence in situ hybridization (FISH) procedures using thermodynamic models." Critical reviews in biotechnology, 2016. **36**(3): p. 566-577.

155. Roca-Cusachs, P., *et al.*, "Stability of microfabricated high aspect ratio structures in poly (dimethylsiloxane)." Langmuir, 2005. **21**(12): p. 5542-5548.

156. Van der Rest, M., *et al.*, "The plasma membrane of Saccharomyces cerevisiae: structure, function, and biogenesis." Microbiological reviews, 1995. **59**(2): p. 304-322.

157. Suzzi, G., P. Romano, and L. Vannini, "Cell surface hydrophobicity and flocculence in Saccharomyces cerevisiae wine yeasts." Colloids and Surfaces B: Biointerfaces, 1994. **2**(5): p. 505-510.

158. Whitesides, G. and A. Stroock, "Flexible methods for microfluidics [J]." Phys Today, 2001. **54**(6): p. 42-48.

159. Martorell, P., A. Querol, and M. Fernández-Espinar, "Rapid identification and enumeration of Saccharomyces cerevisiae cells in wine by real-time PCR." Applied and Environmental Microbiology, 2005. **71**(11): p. 6823-6830.

160. Toldrá, F. and L.M. Nollet, "Advances in food diagnostics." 2017: John Wiley & Sons.

161. Lagally, E., "Microfluidics and Nanotechnology: Biosensing to the Single Molecule Limit." 2014: CRC Press.

162. Zhang, Q., *et al.*, "Microbial detection in microfluidic devices through dual staining of quantum dots-labeled immunoassay and RNA hybridization." Analytica chimica acta, 2006. **556**(1): p. 171-177.

163. Gerdts, G. and G. Luedke, "FISH and chips: Marine bacterial communities analyzed by flow cytometry based on microfluidics." Journal of microbiological methods, 2006. **64**(2): p. 232-240.

164. Sieben, V.J., *et al.*, "An integrated microfluidic chip for chromosome enumeration using fluorescence in situ hybridization." Lab Chip, 2008. **8**(12): p. 2151-2156.

165. Vedarethinam, I., *et al.*, "Metaphase FISH on a chip: Miniaturized microfluidic device for fluorescence in situ hybridization." Sensors, 2010. **10**(11): p. 9831-9846.

166. Zhang, Y., *et al.*, "Single cell analysis of yeast replicative aging using a new generation of microfluidic device." PloS one, 2012. **7**(11): p. e48275.

167. Alvankarian, J., A. Bahadorimehr, and B.Y. Majlis, "A pillar-based microfilter for isolation of white blood cells on elastomeric substrate." Biomicrofluidics, 2013. **7**(1): p. 014102.

168. Li, P.C., *et al.*, "Transport, retention and fluorescent measurement of single biological cells studied in microfluidic chips." Lab Chip, 2004. **4**(3): p. 174-180.

169. Yang, J., *et al.*, "Diffusion characteristics of a T-type microchannel with different configurations and inlet angles." Analytical sciences, 2007. **23**(6): p. 697-703.

170. Loureiro, V.l., "Spoilage yeasts in foods and beverages: characterisation and ecology for improved diagnosis and control." Food Research International, 2000. **33**(3-4): p. 247-256.

171. Rodriguez-Mateos, P., *et al.*, "FISH and chips: a review of microfluidic platforms for FISH analysis." Medical microbiology and immunology, 2020. **209**(3): p. 373-391.

172. Santos, R.S., *et al.*, "Response surface methodology to optimize peptide nucleic acid fluorescence in situ hybridization (PNA-FISH) in Saccharomyces cerevisiae." LWT, 2017. **80**: p. 27-31.

173. Azevedo, A.S., *et al.*, "Optimizing locked nucleic acid/2'-O-methyl-RNA fluorescence in situ hybridization (LNA/2'OMe-FISH) procedure for bacterial detection." PloS one, 2019. **14**(5): p. e0217689.

174. Cerqueira, L., *et al.*, "Establishment of a New PNA-FISH Method for Aspergillus fumigatus Identification: First Insights for Future Use in Pulmonary Samples." Microorganisms, 2020. **8**(12): p. 1950.

175. Bergman, L.W., "Growth and maintenance of yeast", in *Two-hybrid systems*. 2001, Springer. p. 9-14.

Appendix

I. YEPD mediums

Table 2 – Composition of the YEPD medium

Reagent	Concentration	Manufacturer
Yeast extract	1% (w/v)	Merk, Germany
Peptone	2% (w/v)	Liofilchem, Italy
Dextrose	2% (w/v)	Merk, Germany

Table 3 – Composition of the YEPD-agar medium

Reagent	Concentration	Manufacturer
Yeast extract	1% (w/v)	Merk, Germany
Peptone	2% (w/v)	Liofilchem, Italy
Dextrose	2% (w/v)	Merk, Germany
Agar	2% (w/v)	Merk, Germany

II. *Saccharomyces cerevisiae* growth curve

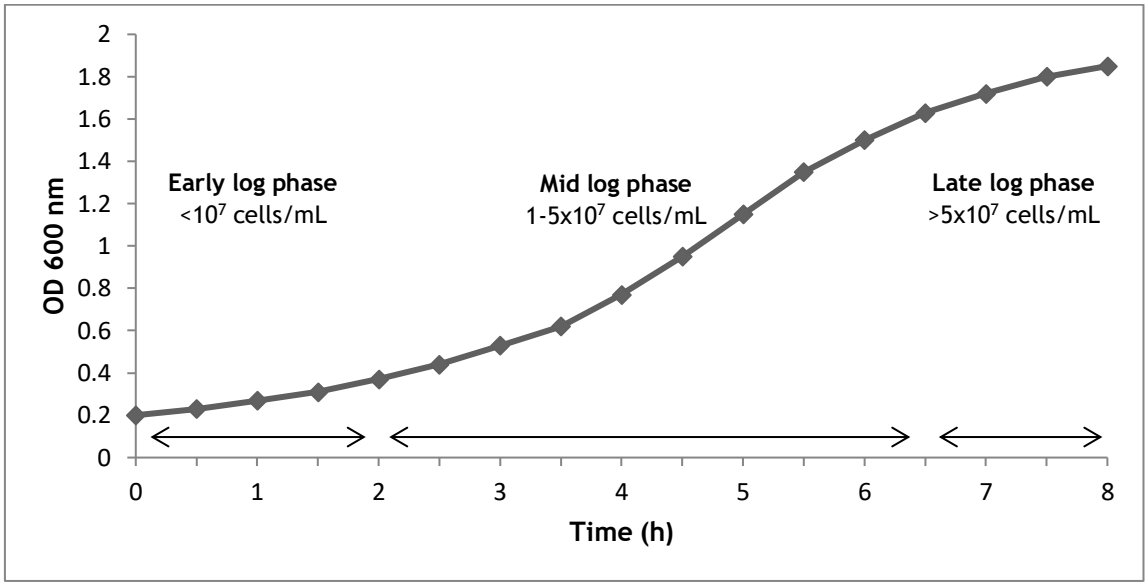

Figure 26 – *Saccharomyces cerevisiae* growth curve and corresponding cell density
Adapted from Lima (2013)[142]. Cell density values from Bergman (2013)[175].

III. FISH solutions

Table 4 – Composition of the PBS solution

Reagent	Concentration	Manufacturer
Sodium chloride	180 nM	Sigma-Aldrich, USA
Sodium phosphate dibasic	9 nM	Sigma-Aldrich, USA
Potassium chloride	3 mM	Sigma-Aldrich, USA
Potassium hydrogen phosphate	1.5 nM	Sigma-Aldrich, USA

Table 5 – Composition of the simplified hybridization solution with PNA (pH 7.5)
For the negative control no PNA probe is added to the hybridization solution.

Reagent	Concentration	Manufacturer
Dextran sulfate	10% (w/v)	Fischer Scientific, UK
PNA probe	200 nM	Panagene Inc, South Korea
Tris-HCl	50 mM	Fischer Scientific, UK
Triton X-100	0.1% (v/v)	Panreac Quimica, Spain

Table 6 – Composition of the washing solution (pH 10)

Reagent	Concentration	Manufacturer
Sodium chloride	15 nM	Sigma-Aldrich, USA
Tris Base	5 mM	Fischer Scientific, UK
Triton X-100	1% (v/v)	Panreac Quimica, Spain

IV. Bending issues in microchannels

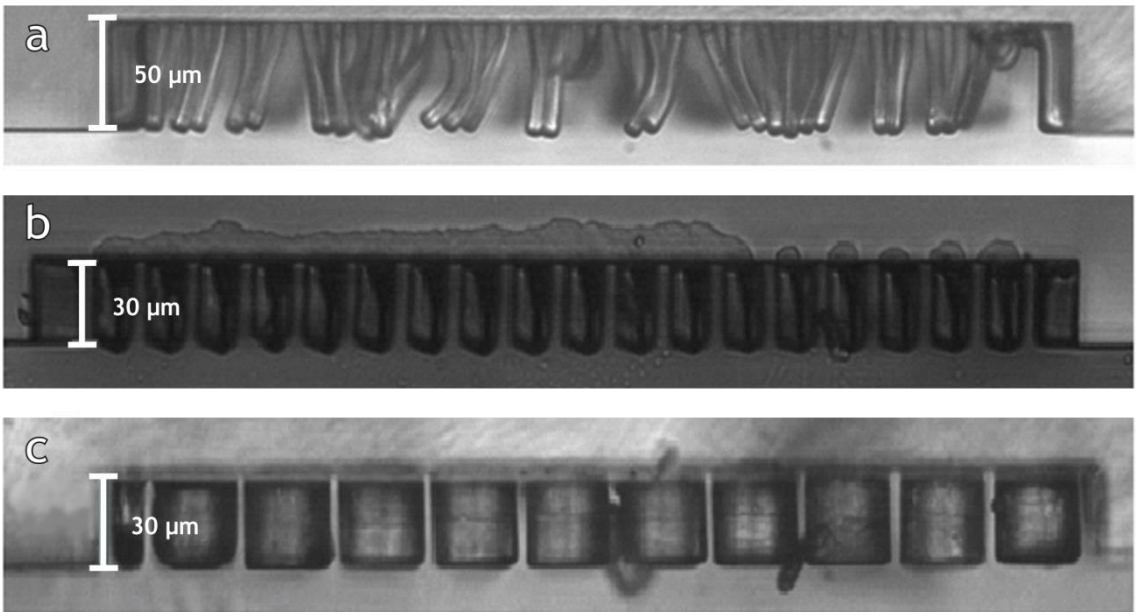

Figure 27 – Cross section and geometrical characterization of microchannels with different depths

(a) Microchannel 2a with 50 µm depth presents bended and missing pillars, creating large gaps that diminish retention capabilities; (b) Microchannel 2b with diamond-based pillars and (c) microchannel 2c with pyramid-based pillars both have a depth of 30 µm, presenting structures with no microfabrication errors and creating the intended 5 µm gaps. These results highlight the importance of designing pillars with self-supporting capabilities, attending to the fact that an increased microchannel depth should require larger pillars. Original magnification 400x. Adapted from Moreira (2014)[15].

V. CFD results for narrow and widened microchannels

Microchannel	Contours of velocity magnitude (m/s)	Streamlines
1a	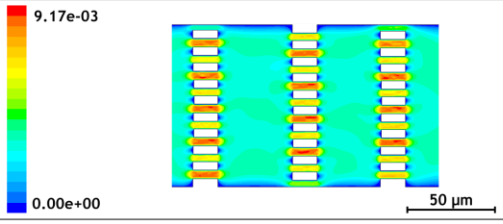	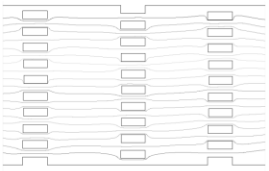
1b (elongated pillar-based)	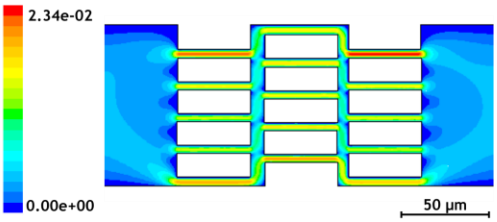	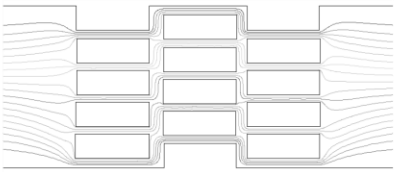
2a	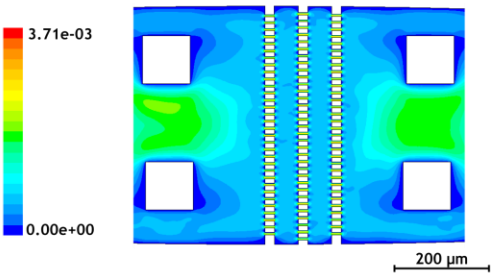	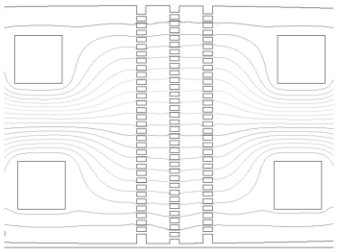
2b (diamond pillar-based)	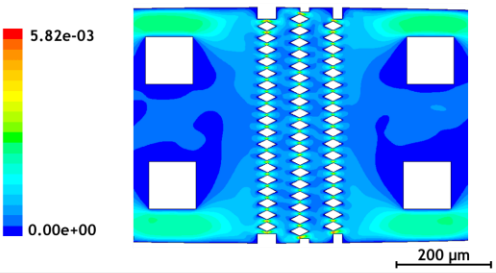	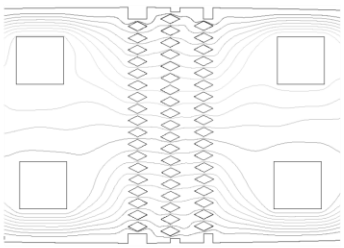
2c (pyramid pillar-based)	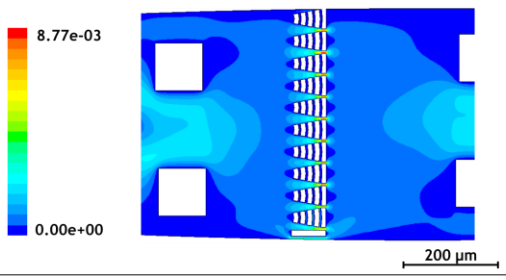	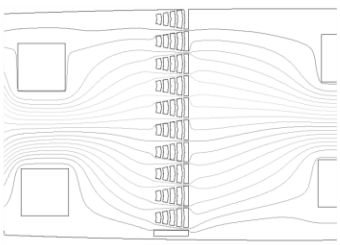

Figure 28 – CFD results for narrow and widened microchannel designs

Velocity magnitude (m/s) and streamlines along the horizontal plane of symmetry.

VI. Removal of non-hybridized probes

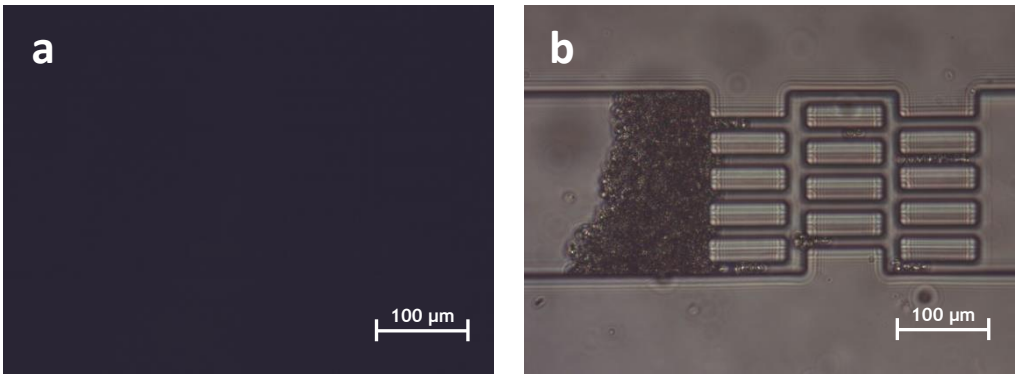

Figure 29 – Efficiency of the washing step to remove non-hybridized PNA probes

(a) By applying PNA-FISH protocol within microfluidic environment with a probe not specific to *S. cerevisiae*, no fluorescence was detected using the FITC filter. (b) The microscope light was turned on to prove that cells were present in the microchannel. Concentration of 10^4 cells/µl. Original magnification 400x.